Orientational phase transitions and the assembly of viral capsids

Sanjay Dharmavaram, Fangming Xie, William Klug, Joseph Rudnick, and Robijn Bruinsma

Phys. Rev. E **95**, 062402 — Published 6 June 2017

DOI: 10.1103/PhysRevE.95.062402

Orientational Phase Transitions and the Assembly of Viral Capsids

Sanjay Dharmavaram[1], Fangming Xie[2], William Klug[3], Joseph Rudnick[1], Robijn Bruinsma[1]
1*Department of Physics and Astronomy, University of California, Los Angeles, CA 90095, USA*
3*Department of Mechanical and Aerospace Engineering,*
University of California, Los Angeles, CA 90095, USA and
2*Department of Physics, University of Science and Technology of China, Hefei, Anhui, China*

We present a Landau theory for large l orientational phase transitions and apply it to the assembly of icosahedral viral capsids. **The theory predicts two distinct types of ordering transitions. Transitions dominated by the $l = 6, 10, 12$ and 18 icosahedral spherical harmonics resemble robust first-order phase transitions that are not significantly affected by chirality.** The remaining transitions depend essentially on including *mixed l states* denoted as $l = 15 + 16$ corresponding to a mixture of $l = 15$ and $l = 16$ spherical harmonics. The $l = 15 + 16$ transition is either continuous or weakly first-order and it is strongly influenced by chirality, which suppresses spontaneous chiral symmetry breaking. The icosahedral state is in close competition with states that have tetrahedral, D_5, and octahedral symmetries. We present a group-theoretic method to analyze the competition between the different symmetries. The theory is applied to a variety of viral shells.

I. INTRODUCTION

The seminal work of Onsager on nematic liquid crystals in the 1940's [1] initiated the theoretical study of *orientational phase transitions*. Orientational phase transitions have since been investigated not only for liquid crystals but also for quasi-crystals, supercooled liquids, metallic glasses, atomic clusters and Fermi liquids [2, 3]. Theories of orientational phase transitions are usually expressed in terms of the orientational order parameter Q_{lm} defined as the coefficient of the spherical harmonic Y_l^m in an expansion of the density $\rho(\Omega)$ of molecules oriented along the solid angle Ω [3]. In Landau theory, the order parameter associated with a continuous phase transition is characterized by a *single* irreducible representations ("irrep") of the symmetry group G_0 of the disordered phase [2]. If G_0 is the group $SO(3)$ of rotations in three dimensions then the order parameter should be characterized by just a single value for l. The remaining $2l+1$ coefficients Q_{lm} of the order parameter must be determined by minimization of a Landau free energy functional expressed as an expansion of the Q_{lm}. The symmetry group G of the ordered phase must be an isotropy subgroup of G_0.

The literature on orientational phase transitions has been mostly restricted to l values less than or equal to $l = 6$, but recently an application of orientational transitions involving larger values of l has emerged in the area of *viral assembly* [5, 6]. Simple viruses are composed of a protein shell – the capsid – that surrounds the viral RNA or DNA genome molecule(s). Fig. 1 shows a cross-section of the reconstruction of a typical small, single-stranded (ss) RNA virus – the flock house virus (FHV) – obtained by X-ray diffraction [7].

According to the Law of Mass Action (LMA) of equilibrium thermodynamics, the self-assembly of an N-monomer structure (such as a capsid) from a monomer-containing solution resembles a first-order phase transition for larger N [8]. Experimental studies appear to confirm the predictions of the LMA for the case of the assembly of *empty* capsids [9]. In terms of kinetics, empty capsid assembly has been described as a diffusion-limited "protein-by-protein" nucleation-and-growth process where capsid proteins diffuse in from infinity towards partially assembled protein shells [10, 11]. Diffusion-limited assembly of complete viruses encapsidating ss RNA genome molecules should be enhanced by the presence of the genome molecule [12]. However, recent experiments [13] indicate that viral assembly in the presence of the genome molecule also can have the character of the *cooperative ordering* of a disordered protein-RNA precursor condensate [14], as shown in Fig. 2. Assembly is not diffusion-limited in this case. Numerical simulations of capsid assembly by Hagan [15] have encountered both scenarios. This second assembly mode is the focus of the current paper.

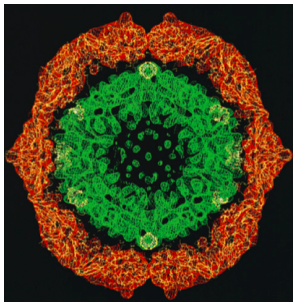

FIG. 1. Cross-section of a reconstruction of the flock house virus as obtained by x-ray diffraction viewed along a two-fold icosahedral axis (J.Johnson, private communication). Red: capsid composed of 180 identical proteins. Green: enclosed, single-stranded RNA genome molecule (online in color). The diameter is 35 nanometers.

A theory for the cooperative ordering transition of a shell of capsid proteins on the surface of a condensed ss RNA globule may be cast in the language of a theory of an orientational transition by identifying $\rho(\Omega)$ with the

capsid mass density per unit area on a spherical surface along a direction Ω. The direction is measured from the center of a sphere of radius R, which we identify as the inner radius of the assembled capsid (see Fig. 2).

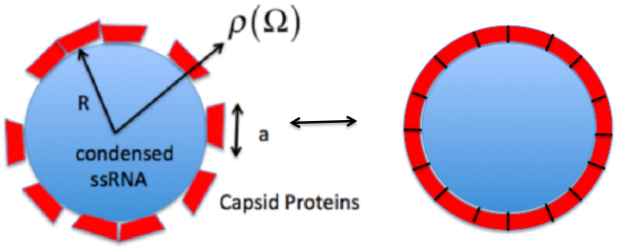

FIG. 2. Viral assembly by the solidification of a liquid-like precursor state (left) in the form of a condensate of single-stranded RNA material and groups of capsid proteins. The condensate has a radius R while the basic structural units composed of one or more proteins have a characteristic size a. The mass density of the structural units in a direction Ω is given by $\rho(\Omega)$.

The free energy of a Landau theory of orientational transitions is a functional of $\rho(\Omega)$. This primary order-parameter density should be viewed as a *coarse-grained* density distribution of either the capsid proteins or of groups of capsid proteins that are present in the disordered precursor state as relatively stable entities (see Section V). The full density profile, as measured for example in electron microscopy or X-ray diffraction studies, must be constructed by distributing the proteins, or groups of proteins, in conformity with $\rho(\Omega)$. As discussed in Section V, inclusion in the theory of more of the internal structure of the capsid proteins requires additional "secondary" order parameters whose values would have to be determined by more complex density functionals whose terms would have to vary from virus to virus, The Landau free energy of the primary order parameter constructed form symmetry arguments can be expected to represent only more universal aspects.

In the disordered phase $\rho(\Omega)$ is a constant (equal to $1/(4\pi)$) while in the ordered phase it acquires a density modulations on a length scale a that is of the order of the size of the molecular groups in the precursor state. If $\rho(\Omega)$ is expanded in spherical harmonics Y_l^m then the characteristic value of l should be of the order of R/a. This is in the range of $10-30$ and thus considerably larger than the l values encountered in most earlier studies of orientational ordering [2].

If one restricts the expansion of $\rho(\Omega)$ to a single value of l in accordance with the tenets of Landau theory, then the icosahedral density modulations can be directly obtained by requiring $\rho(\Omega)$ to be invariant under the actions of the icosahedral group I. For given l, the resulting linear combination of spherical harmonics Y_l^m are well known as the *icosahedral spherical harmonics*, denoted by $\mathcal{Y}_h(l)$ [16]. Icosahedral spherical harmonic can be constructed for even values only if l is given by $l = 6j+10k$ with $j, k \in \{0, 1, 2, \cdots\}$ and for odd values of l if $l = 15 + 6j + 10k$ [17]. For even l less than 14, this restricts l to $6, 10, 12$ while there are no restriction for larger even l. Odd l icosahedral states are restricted to $l = 15, 21, 25, 27$ for l less than 29 while there are no restrictions for larger odd l.

The lowest l value that allows construction of an icosahedral shell is thus $l = 6$. The properties of the $l = 6$ orientational phase transition have already been extensively explored in the context of quasi-crystals and glasses [3, 18]. A conventional first-order phase transition separates the uniform state from a stable, $l = 6$ icosahedral state. The reason the transition is first-order is because of the presence of a non-zero cubic term in the Landau free energy. The $l = 6$ icosahedral state competes with states that have different symmetries, but it is stable over a substantial sector of parameter space.

Could the $l = 6$ icosahedral orientational transition be viewed as a model for Landau theories of the assembly of viral capsids? Like all proteins, those comprising a capsid (which are known as "subunits") are chiral molecules that lack an inversion center. X-ray diffraction and electron microscopy reconstructions of viral capsids sometimes display a pronounced chiral character [19]. However, $\mathcal{Y}_h(6)$ is even under inversion, as are all even icosahedral spherical harmonics. For this reason, all even l icosahedral spherical harmonics were excluded from the current Landau theory of viral assembly [5, 6]. The absence of inversion symmetry is also the reason that the symmetry group G_0 of the disordered phase is $SO(3)$ rather than $O(3)$. The lowest *odd* icosahedral spherical harmonic is $l = 15$. This should correspond to the smallest icosahedal viral shells.

Fig. 3A shows a reconstruction of the capsid of the parvovirus [20] viewed along a 5-fold symmetry and compares it $\mathcal{Y}_h(15)$ (Fig. 3B). The parvovirus belongs to the $T = 1$ class, which includes the smallest icosahedral viruses composed of 60 proteins (though larger viruses, such as the picornavirus, also may be classified as $T = 1$). The $\mathcal{Y}_h(15)$ icosahedral spherical harmonic indeed reproduces the large-scale features of the capsid. Note that both have a chiral character. Reversing the sign of the $\mathcal{Y}_h(15)$ density produces a new density profile that cannot be transformed into the old density profile by a rotation. There are thus two isomeric densities that correspond to $\mathcal{Y}_h(15)$, which is not the case for $\mathcal{Y}_h(6)$. The $\mathcal{Y}_h(15)$ density goes to zero at the 5-fold symmetry sites, which is true for odd l spherical harmonics in general. A systematic comparison of other viral capsids and the odd-l icosahedral spherical harmonics can be found in refs. [5, 6]. Larger viruses are associated with $\mathcal{Y}_h(l)$ with larger odd l. For example, the intensely-studied CCMV virus, discussed more in Section V, is associated with $\mathcal{Y}_h(27)$.

The *cubic* non-linear terms in the Landau free energy vanishes for a density represented by $\mathcal{Y}_h(l)$ with l

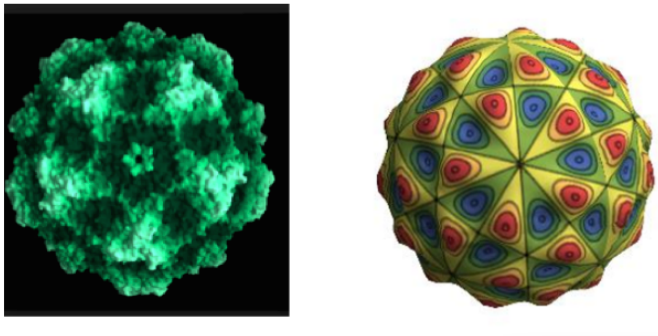

FIG. 3. A) Reconstruction of the *parvovirus*, viewed along a 5-fold symmetry axis (from ref.[a]). B) The $\mathcal{Y}_h(15)$ icosahedral spherical harmonic.

[a] http://www.virology.net/BigVirology/BVDNAparvo.html

odd. This, in turn, means that cooperative viral assembly should always be a *continuous* transition, at least in mean-field theory [21]. This is in contrast with the protein-by-protein capsid assembly scenario that encounters equilibrium activation energy barriers that are estimated to be large compared to the thermal energy [10].

One problem with the notion that cooperative assembly might be a continuous transition is that in the limit that the sphere radius goes to infinity, the solidification of chiral molecules on a spherical surface should reduce to the solidification of an infinite layer of chiral molecules but liquids composed of chiral molecules undergo conventional, first-order discontinuous solidification transitions [22]. Resolving whether capsid assembly is a continuous or a discontinuous transition is one of the motivations of the paper.

It should be noted that transitions between different states of a capsid are not true phase transitions. If, for example, a capsid can exist in competing liquid and positionally ordered states with respective free energies F_l and F_s then this should be interpreted as stating that in a solution the concentration ratio N_s/N_l of capsids in solid, respectively, liquid states equals $\exp(-(F_s - F_l)/k_BT)$. Viral capsids have free energies in the range of $10^3 k_BT$ so if $(F_s - F_l)$ changes sign as a function of some parameter then there will be relatively sharp kink in the dependence of the concentration ratio on this parameter but there is not a true phase transition. In the following, the use of the word "transition" should be interpreted in this sense.

In a recent letter [23] we showed that the $\mathcal{Y}_h(15)$ state is thermodynamically unstable in linear stability analysis but that stability can be regained by including mixing between the $l = 15$ and $l = 16$ states. The order parameter is then a pair of coefficients that provides the weights of the $\mathcal{Y}_h(15)$ and $\mathcal{Y}_h(16)$ components. An unphysical feature of the achiral theory is the presence of spontaneous chiral symmetry breaking and the absence of chirality in the uniform and even l icosahedral states. Chirality was included as the lowest-order pseudo-scalar term in the free energy density rather then as a selection rule imposed on the achiral Landau theory [5, 6].

The aim of the present paper is to determine the nature of the structures that compete with the icosahedral states and to propose a systematic group-theoretic framework for constructing stability diagrams. The linear stability analysis of icosahedral states for the achiral Landau free energy is reviewed in sections II A and B. In section II C, we develop the group-theoretic formalism that relates the instabilities to irreducible representations of the icosahedral group. In section III we review the results of numerical searches for the competing non-icosahedral states, using again group theory as a guide, and construct the stability diagrams. Achiral Landau theory by itself produces unphysical results, such as the appearance of spontaneous chiral symmetry breaking transitions. This is corrected in section IV where we first present a method for the systematic construction or pseudoscalar invariants and then demonstrate that when the lowest-order pseudo-scalar invariant is included the uniform and stable even l states acquire chirality. In sections IV B and IV C, we treat the effect of chirality on the mixed $l = 15+16$ state and show that it removes the unphysical chiral symmetry breaking transition. We conclude in section V with a discussion of the predictions of the theory for a number of different viruses.

II. ACHIRAL LANDAU-BRAZOVSKII FREE ENERGY.

Our starting point is the Landau-Brazovskii (LB) free energy expression for "weak" solidification, which has been used to describe ordering transitions in liquid crystals, block co-polymers and other soft-matter systems [2, 24]. The defining feature of a LB free energy is the fact that the static structure factor $S(q)$, as obtained from the quadratic terms in the free energy density, has a maximum at some $|\vec{q}| = k_0$ that diverges at a critical value of a control parameter. The version of the LB free energy $\mathcal{H}_{LB}$ that we use is defined by the free energy density

$$\mathcal{H}_{LB} = \int \left(\frac{1}{2}\Big((\Delta + k_0^2)\rho\Big)^2 + \frac{r}{2}\,\rho^2 + \frac{u}{3}\,\rho^3 + \frac{v}{4}\,\rho^4 \right) dS. \tag{1}$$

(with $k_BT = 1$). The integral is over the surface of a sphere of radius R. The Δ in the first term is the Laplace-Beltrami operator defined on the spherical surface while k_0 is the characteristic wavenumber of the density modulation of the ordered state. For the present case, k_0 can be estimated as 2π divided by the size a of the proteins or protein groups present in the liquid-like precursor state. The next three terms constitute a Taylor expansion of the free energy density in powers of ρ, with r, u, and v expansion coefficients. If one retains only the quadratic terms

in the free energy, then the structure factor $S(q) = \langle |\rho_q|^2 \rangle$ is proportional to $1/[(k_0^2 - q^2)^2 + r]$ in the large R limit. As required, $S(q)$ has a maximum at $q = k_0$ that diverges in the limit that the control parameter r goes to zero.

In the large R limit, the minimization of this LB free energy produces a phase diagram that contains, apart from the uniform state, a hexagonal two-dimensional (d=2) crystal and a d=2 lamellar phase [25]. We will focus here on the transition line between the hexagonal and isotropic phases. The hexagonal solid is represented as the superposition of three density waves with wavevectors of magnitude k_0 oriented at 120^o with respect to each other. For positive v and non-zero u, this leads for decreasing r to a first-order phase transition from a state with $\rho = 0$ to a state with non-zero ρ.

The condition for a density modulation to constitute an extremum of the LB free energy is that the first functional derivative $\frac{\delta H_{LB}(\rho)}{\delta \rho}$ must vanish. This leads to the Euler-Lagrange equation

$$\frac{\delta \mathcal{H}_{LB}(\rho)}{\delta \rho} = (\Delta + k_0^2)^2 \rho + r\rho + u\rho^2 + v\rho^3 = 0. \qquad (2)$$

As discussed in Section I, if the uniform phase is known to be invariant under the group SO(3) of rotations in three dimensions then Landau theory instructs us that, sufficiently close to a continuous transition, the density modulation can be associated with a single irrep of SO(3). It follows that the density modulation is expandable in spherical harmonics belonging to a particular l value. The collection of $2l + 1$ numbers c_m in the expansion

$$\rho(\Omega) = \sum_{m=-l}^{l} c_m {Y_l}^m(\Omega) \qquad (3)$$

collectively constitute the orientational order parameter. The condition that the density is real imposes the additional constraint $c_m^* = (-1)^m c_{-m}$. Under these conditions, the LB free energy simplifies to

$$\mathcal{H}_{LB}([c_m])/R^2 = \int \left(\frac{t_l}{2}\rho^2 + \frac{u}{3}\rho^3 + \frac{v}{4}\rho^4 \right) d\Omega. \qquad (4)$$

Here, $t_l = r + [(k_0 R)^2 - l(l+1)]^2/R^4$ while the integral is over solid angles Ω. The quantity t_l is the effective reduced temperature for icosahedral ordering in this subspace. The optimal l value is the one that minimizes t_l for given $k_0 R$. This leads to $l \simeq k_0 R$ so the preferred l value increases linearly with the shell radius R. We now can divide the $k_0 R$ axis into segments $l^2 < k_0 R^2 < (l+1)^2$ so that in each segment the associated t_l changes sign with decreasing r before any of the other t_l. For example, condensation is dominated by the $l = 15$ subspace if $(k_0 R)^2$ lies in the interval $15 < (k_0 R)^2 < 16$.

Inserting the expansion for $\rho(\Omega)$ in spherical harmonics into Eq. 4 produces a quartic polynomial in the $2l + 1$ expansion coefficients c_m. Formal minimization leads to the condition that the $2l + 1$ projections of the Euler-Lagrange equation on the spherical harmonic Y_{lm} must be zero:

$$\langle Y_l^m, \frac{\delta \mathcal{H}_{LB}(\rho)}{\delta \rho} \rangle = G_m([c_m]) = 0, \ -l \le m \le l. \qquad (5)$$

where the $G_m([c_m])$ are a set of $2l+1$ cubic polynomials in the c_m. The polynomials can be obtained from the *Sattinger algorithm* [26], which uses the ladder operators of quantum mechanics as generators of the Lie algebra of $SO(3)$ in order to generate the most general polynomials in the $2l + 1$ variables $(c_{-l}, \cdots, c_0, \cdots, c_l)$ that are $SO(3)$-equivariant. One only needs to compute as many integrals of products of spherical harmonics as are required to obtain the coefficients that are left undetermined by the Sattinger algorithm. Alternatively, one can also use the Wigner matrices [27] for integrals over products of spherical harmonics.

Once a solution has been found, thermodynamic stability in the fixed l subspace requires that the eigenvalues of the $(2l + 1)$ times $(2l + 1)$ stability matrix $\langle Y_l^m | \frac{\delta^2 \mathcal{H}_{LB}}{\delta \rho^2} | Y_l^{m'} \rangle$ (or "Hessian") are positive apart from three zero eigenvalues that correspond to global rotations over the three Euler angles.

A. Icosahedral Free Energy Extrema: odd l

First consider the odd l icosahedral spherical harmonics. The smallest odd l value that supports an icosahedral state $l = 15$. The invariant icosahedral density is proportional to $\mathcal{Y}_h(15)$ where

$$\begin{aligned} \mathcal{Y}_h(15) \propto & \frac{3003}{625} Y_{15}^{-15}(\theta,\phi) - \frac{33}{625}\sqrt{15834}\mathcal{Y}_{15}^{-10}(\theta,\phi) \\ & - \frac{3}{125}\sqrt{\frac{667667}{5}} Y_{15}^{-5}(\theta,\phi) - \frac{3}{125}\sqrt{\frac{667667}{5}} Y_{15}^{5}(\theta,\phi) \\ & + \frac{33}{625}\sqrt{15834} Y_{15}^{10}(\theta,\phi) + \frac{3003}{625} Y_{15}^{15}(\theta,\phi) \end{aligned} \qquad (6)$$

Note that only 6 of the 31 coefficients are non-zero and that the non-zero m terms are multiples of 5 [28]. This makes sense given that an icoshedral density profile density must have five-fold symmetry axes. The three-fold symmetry axes of the icosahedron are not evident in this expression because of the choice of the z-axis for the m indices, which lies along a five-fold axis. Acting on the above expression with a rotation operator that places the z-axis along one of the three-fold symmetry axes, would highlight three-fold symmetry. There are 31 coupled equations $\langle Y_{15}^m, \frac{\partial \mathcal{H}_{LB}}{\partial \rho} \rangle = 0$ for the c_m. The equations are solved for the c_m corresponding the coefficients of $\mathcal{Y}_h(15)$ in Eq. 6. The density associated with the $l = 15$ icosahedral spherical harmonic is thus an extremum of the LB free energy restricted to the $l = 15$ sector.

Denote the remaining undetermined overall multipica-

tive factor of $\mathcal{Y}_h(15)$ by ζ. Inserting this in the LB free energy and setting the derivative with respect to ζ to zero leads to the equation:

$$\zeta\left(t_{15} + 0.789v\zeta^2\right) = 0, \tag{7}$$

where we set $(k_0R)^2 = 15 \times 16$ in the middle of the $l = 15$ stability segment. This equation now has the standard form of a second-order Landau phase transition. For $t_{15} > 0$, the solution is $\zeta = 0$ while for $t_{15} < 0$ there are two degenerate solutions: $\zeta = \pm 1.126\frac{\sqrt{-t_{15}}}{\sqrt{v}}$. The solution pair is related by inversion. The onset of an $l = 15$ icosahedral density modulation thus involves spontaneous chiral symmetry breaking. The two solutions will be denoted by D (from dextro) for the plus sign and L (from laevo) for the minus sign.

However, as reported earlier [23], when the eigenvalues of the 31×31 stability matrix for the $l = 15$ state are computed numerically, one finds that the icosahedral state has one three-fold degenerate negative eigenvalue and one four-fold degenerate negative eigenvalue. Similar instabilities are encountered also for the subsequent odd l icosahedral states $l = 21$, $l = 25$, and $l = 27$. For example, the icosahedral spherical harmonic $\mathcal{Y}_h(25)$ has a stability matrix with 51 eigenvalues, 27 of which are negative!

The appearance of negative eigenvalues for $l = 15$ can also be demonstrated directly. Perturb about the icosahedral state $\rho = \zeta\mathcal{Y}_h(15) + \hat{\rho}$ with the perturbation $\hat{\rho}$ restricted to the space of $l = 15$ spherical harmonics. The change $\delta\mathcal{H}$ introduced by the perturbation is

$$\delta\mathcal{H}/R^2 = \int \left(\frac{t_{15}}{2}\hat{\rho}^2 + |t_{15}|\frac{3}{2}(1.126)^2\mathcal{Y}_{15}^2\hat{\rho}^2\right)\, d\Omega. \tag{8}$$

up to quadratic order in $\hat{\rho}$. Try $\hat{\rho} = Y_{15}^0$. By direct integration of (8) one obtains $\delta\mathcal{H} = -0.003261|t_{15}|$, which holds for any non-zero value of w. Since δH is negative, the icosahedral state is indeed unstable.

We have numerically searched the space spanned by the 31 expansion coefficients c_m in the $l = 15$ subspace without imposing icosahedral symmetry. We searched for locally stable minima using the FindMinimum subroutine of Mathematica with randomized initial conditions. Once a minimum was identified, the Newton-Raphson method was applied for further refinment. The minimum with the lowest free energy obtained in this manner is shown in Fig. 4. It is a non-icosahedral structure with only a single five-fold symmetry axis. In addition, there are five quasi two-fold axes at 90 degrees. This density corresponds to one of the two one-dimensional irreducible representation of the dihedral group D_5, a subgroup of the icosahedral group I [4].

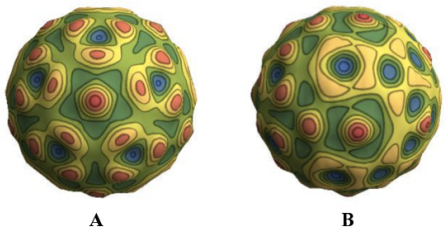

FIG. 4. Minimum free energy state in the $l = 15$ sector for $t_{15} = -0.1$ and $v = 10$. A: View along the single 5-fold symmetry axis. B: View perpendicular to the 5-fold axis along a quasi two-fold axis.

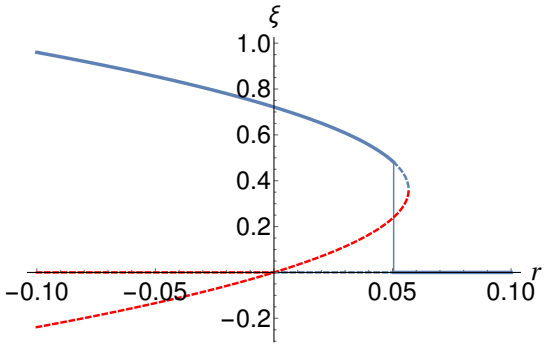

FIG. 5. Solution of Eq. 9 with the order-parameter amplitude ξ as a function of r the instability control parameter. The k_0 parameter is set at the optimal value $k_0^2 = 6 \times 7$ for the $\mathcal{Y}_h(6)$ icosahedral spherical harmonic. Stable solution branches are shown as a solid blue line, metastable branches as a dashed blue line. Solution branches with one or more negative eigenvalues are shown as a dashed red line.

B. Icosahedral Free Energy Extrema: even l

It is also useful to examine even l icosahedral spherical harmonics. The lowest even l value is the well-studied $l = 6$, with associated icosahedral spherical harmonic $\mathcal{Y}_h(6) = Y_{0,0} + \sqrt{\frac{7}{11}}Y_{6,5} - \sqrt{\frac{7}{11}}Y_{6,-5}$ [29]. Only three of the 13 coefficients c_m are non-zero. The 13 coupled equations $G_m([c_m]) = 0$ for the expansion coefficients are solved by these c_m, which confirms that the icosahedral state is again an extremum of the LB free energy. If we denote the undetermined overall multiplicative factor of $\mathcal{Y}_h(6)$ by ξ, insert the Ansatz $\rho_I = \xi\mathcal{Y}_h(6)$ into the free energy and minimizing the free energy with respect to ξ, one obtains:

$$r\xi + \tilde{u}\xi^2 + \tilde{v}\xi^3 = 0, \tag{9}$$

with $\tilde{u} = u(50\sqrt{13}/323\sqrt{\pi})$ and $\tilde{v} = 2145v/(1564\pi)$ for $(k_0R)^2 = 6 \times 7$, so in the middle of the $l = 6$ stability segment. This equation has the standard form for a first-order Landau phase transition. Fig. 5 shows the order-parameter amplitude ξ as a function of r. Solution branches for which the 13×13 stability matrix has pos-

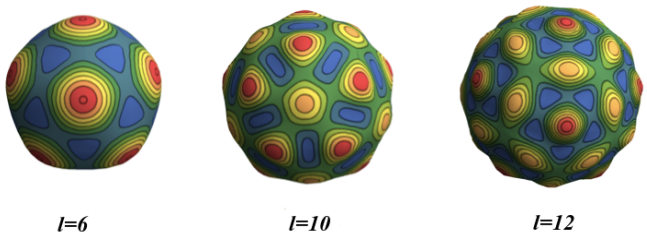

FIG. 6. Stable icosahedral density profiles for $l = 6$, 10 and 12. In all three cases, the five-fold symmetry sites are density maxima for our choice of the sign of u. This holds for all even l icosahedral spherical harmonics.

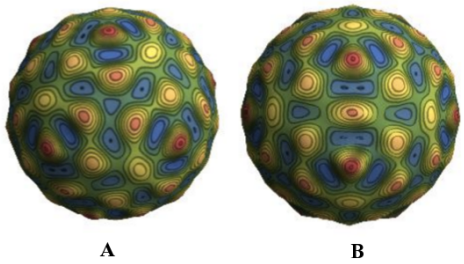

FIG. 7. Tetrahedral free energy minimum in the $l = 16$ sector for $t_{16} = -0.1$ and $v = 10$ A: View along a 3-fold symmetry axis. B:

itive eigenvalues plus three zero eigenvalues are shown as solid and dashed blue lines. The solid blue line is the minimum free energy state. The onset of icosahedral order as a function of r proceeds via a first-order transition with an order parameter discontinuity. The dashed red curve represents a solution for which the Hessian has negative eigenvalues, indicating that this is a first-order transition with metastability. The stability of the $l = 6$ state is consistent with the earlier work [3, 18]. Stable icosahedral states were found also for $l = 10$, $l = 12$, and $l = 18$. The first three stable icosahedral density modulations are shown in Fig. 6.

This exhausts the list of stable icosahedral spherical harmonics. The Hessian of the $l = 16$ icosahedral state has negative eigenvalues however. We carried out a numerical search for a minimum in the $l = 16$ sector as we did for $l = 15$. The lowest stable minimum energy structure we found is shown in Fig. 7. The resulting structure has eight three-fold axes and the symmetry of a one-dimenisonal irrep of the tetrahedral subgroup T of both the icosahedral and the octahedral groups. (See Figs. 7A and B). The three-fold axes display chirality. Choosing the four of those axes with the same chirality to be the locations of vertices generates one tetrahedron. Choosing the four axes with the opposite chirality generates a tetrahedron that is dual the the first one. This same structure has been found earlier by Matthews [4] in a study of the even l spherical harmonics.

C. Group theory.

So far we used the $2l + 1$ spherical harmonics Y_l^m as the basis, which indeed is the natural basis for examining symmetry breaking of the uniform state with $SO(3)$ symmetry. It is not however a convenient basis for examining symmetry breaking of an icosahedral state, as encountered in the previous subsection. In order to classify the instabilities of the $l = 15$ and $l = 16$ icosahedral states, we will reorganize the expansion basis. For that purpose, we construct a new basis composed of groups of linear combinations of Y_l^m that transform according to the different irreps of I under the symmetry operations of I.

The icosahedral group has five irreps with the character table shown below [30, 31]. The notation for the

TABLE I. Character table for the five irreducible representations of the icosahedral group

	E	$\mathcal{C}_5, \mathcal{C}_5^4$	$\mathcal{C}_5^2, \mathcal{C}_5^3$	$\mathcal{C}_2$	$\mathcal{C}_3, \mathcal{C}_3^2$
A_g	1	1	1	1	1
F_{1g}	3	$\frac{1}{2}(1+\sqrt{5})$	$\frac{1}{2}(1-\sqrt{5})$	-1	0
F_{2g}	3	$\frac{1}{2}(1-\sqrt{5})$	$\frac{1}{2}(1+\sqrt{5})$	-1	0
G_g	4	-1	-1	0	1
H_g	5	0	0	1	-1

rotational symmetry operations $\mathcal{C}_j$ of I is detailed in Appendix A. The second column, which contains the characters associated with the identity E, also gives the dimension d of the irrep. Using this character table, one can project any spherical harmonic Y_l^m onto an irrep i of I:

$$\sum_{j=1}^{5} \chi_i^{(j)} \sum_{\mathbf{R}\in C_j} Y_l^m(\mathbf{R}(\widehat{r})) \tag{10}$$

Here, $\mathbf{R}$ is one of the 60 symmetry operations of I while j runs over the five entries of the appropriate row of the character table. A rotated spherical harmonic $Y_l^m(\mathbf{R}(\widehat{r}))$ can be expanded in terms of the $2l+1$ unrotated spherical harmonics with the same l:

$$Y_l^m(\mathbf{R}(\widehat{r})) = \sum_{m'=-l}^{m'=+l} [D^l_{mm'}]^* Y_l^{m'}(\widehat{r}) \tag{11}$$

where $[D^l_{mm'}]^*$ is the complex conjugate of an element of the (tabulated) Wigner D-matrix [27]. By applying this projection method to any of the $2l+1$ spherical harmonics, one obtains five linear combinations of the spherical harmonics corresponding to the five irreps of I, generating in total a set of five times $2l + 1$ combinations. This set is over-complete and in some cases the operation in Eq. (10) produces a vanishing result. By diligently sift-

ing through this set and extracting all linearly independent terms, one can construct of a new orthonormal basis composed of $2l+1$ real basis states $\phi_i^{(j)}(\theta,\phi)$. The subscript i again refers to the irrep, while the superscript j in parentheses runs over the d-dimensional basis *within* for that representation. For example, j runs from 1 to 3 for irrep F_{1g}. The normalization is

$$\int_0^{\pi}\int_0^{2\pi}\phi_i^{(j)}(\theta,\phi)^2\sin(\theta)d\phi\,d\theta = 1 \tag{12}$$

The basis function corresponding to the one dimensional irrep A_g remains the familiar $\mathcal{Y}_h(l)$, which can be explicitly constructed by this route. In Appendix A we illustrate the method for the familiar case of $l=6$.

D. $l = 15$

Applying this method to the $l=15$ case, one obtains one instance of the one-dimensional irrep (A_g or $\mathcal{Y}_h(15)$) two instances of each of the three dimensional representations (F_{1g} and F_{2g}), two instances of the four dimensional representation G_g and two instances of the five dimensional representation H_g. This yields a total number of new basis states equal to $1\times1+2\times3+2\times3+2\times4+2\times5 = 31$ that equals to $2l+1$ as required for a complete basis.

Start by allowing only the one-dimensional irrep A_g. Including non-linear terms, the LB free energy takes the form

$$\frac{1}{2}t_{15}\zeta^2 + \frac{0.789}{4}v\zeta^4 \tag{13}$$

As discussed below Eq., this predicts a continuous transition to an ordered $l=15$ icosahedral state at the point $t_{15}=0$. Now allow the other 30 basis functions to participate in the Hamiltonian but include their expansion coefficients only to quadratic order. The resulting Hamiltonian is then diagonal in terms of these expansion coefficients plus ζ. Diagonal entries are the same for the basis states of a given irrep. We define $t_i(k)$ to be the quadratic coeffcient for the instance k that irrep i is realized.

Table II lists the t_is: All coefficients are proportional to the effective temperature t_{15} of the one-dimensional irrep A_g shown in the first row. The zero in the second row for one of the F_{1g} corresponds to the three zero eigenvalues associated with rotation, as mentioned earlier. Instabilities are associated with negative values for $t_i(k)$. The first one is a three-fold instability associated with F_{2g} while the second one is a a four-fold instability associated with G_g so together there are seven negative eigenvalues.

The new basis is complete in the $l=15$ space but for it to be an *economical* basis for the present case, the structure shown in Fig. 4 should be the superposition of the one-dimensional representation A_g plus a small number of densities that transform according to the higher dimensional irreps. In the simplest case, those would be the two irreps with negative t_i. We find that the structure of Fig. 4 is a linear superposition of A_g plus one copy each of the four d=3 irreps $F_{1g}(k=1,2)$ and $F_{2g}(k=1,2)$. In each case, one must pick an eigenvector with 5-fold symmetry. All four of the five-fold axes must be aligned with one of the 5-fold axes of A_g. The d=4 irrep G_g does not appear to contribute. Group theory thus indicates that Fig. 4 can be viewed a distorted $l=15$ icosahedral structure. The expectation that only irreps with negative t_i should be present in the final structure is, however, wrong. As noted previously, this state also corresponds to the one-dimensional A_2 irrep of the dihedral group D_5.

TABLE II. Quadratic coefficients t_i for the nine instances of irreps of the icosahedral group for $l=15$. The relationships hold when $t_{15}<0$

Irreducible representation	Quadratic coefficient, $t_{15,i}$
$t_{A_g}(k=1)$	$2\|t\|_{15}$
$t_{F_{1g}}(k=1)$	0
$t_{F_{1g}}(k=2)$	$0.016385\|t_{15}\|$
$t_{F_{2g}}(k=1)$	$-0.0184816\|t_{15}\|$
$t_{F_{2g}}(k=2)$	$0.00332569\|t_{15}\|$
$t_{G_g}(k=1)$	$-0.00239087\|t_{15}\|$
$t_{G_g}(k=2)$	$0.0429669\|t_{15}\|$
$t_{H_g}(k=1)$	$0.335413\|t_{15}\|$
$t_{H_g}(k=2)$	$0.0618115\|t_{15}\|$

E. $l = 16$

When the same analysis is carried out for $l=16$, the lowest even l icosahedral structure that is unstable, one encounters one instance of the one dimensional representation, A_g, corresponding to $\mathcal{Y}_h(16)$, two instances of the three dimensional representation F_{1g}, one instance of the three dimensional representation F_{2g}, two instances of the four dimensional representation G_g and three instances of the five dimensional representation H_g. The total number of basis states is $1\times1+2\times3+1\times3+2\times4+3\times5=33$, which equals $2l+1$ as required. Restriction to the one dimensional representation leads to the free energy expression whose extrema correspond to solutions of Eq. (9). If the cubic coefficient is equal to zero then there is a continuous ordering transition as t_{16} passes through zero, and the ordered state is quadratically stable. However, when the third order coefficient is non-zero the ordered state acquires instabilities. Fig. 8 is a plot of quadratic coefficients: Two of the curves lie below the horizontal axis and correspond to instabilities, one of them to a three dimensional irrep and the other to a four dimensional irrep. One of the curves lies along the horizontal axis, corresponding to a three dimensional irrep and reflecting the rotational invariance of the energy

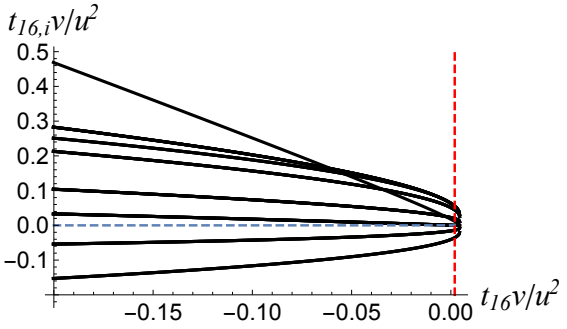

FIG. 8. The quadratic coefficients, $t_{16,i}$ when there is ordering for $l = 16$. The nine curves correspond to the nine irreducible representations comprising the basis set (one one dimensional, three three dimensional, two four dimensional and three five dimensional). The dashed horizontal curve along the axis $t_{16,i}v/u^2 = 0$, corresponds to one of the three dimensional representations that reflects the rotational invariance of the energy of the condensed state. The vertical dashed line indicates the onset of the first order transition to ordering at $t_{16} \simeq 0.002u^2/v$. All curves terminate at the far right, corresponding to the onset of a local non-zero minimum in the free energy at $t_{16} \simeq 0.004u^2/v$.

of the condensed state.

This basis set applied to the decomposition of the $l = 16$ structure shown in Fig. 7 does *not* provide an economic description. Alternatively, Fig. 7 can be shown to comport with the symmetry of the *octahedral group*. The octahedral group is composed of the 24 rotations that leave the octahedron—or its dual regular polyhedron, the cube—unchanged. This group has five irreducible representations, the character table of which is shown in Table III. In the case of this group there

TABLE III. The character table of the octahedral group. As in the case of Table I, the number in the second second column is the dimensionality of the representation.

Irrep	E	$\mathcal{C}_3(8)$	$\mathcal{C}_2(3)$	$\mathcal{C}_2(6)$	$S_4(6)$
A_1	1	1	1	1	1
A_2	1	1	1	-1	-1
E	2	-1	2	0	0
F_2	3	0	-1	1	-1
F_1	3	0	-1	-1	1

are two one dimensional irreps. The first,A_1, is invariant under the action of rotations that leave the octahedron unchanged. The second, A_2, is either transformed into itself or minus itself under such a rotation.

For the case of $l = 16$ there are two instances of the irrep A_1 and one instance of A_2, as well as three of the two dimensional irrep E and four each of F_1 and F_2, for a total of $2\times1+1\times1+3\times2+4\times3+4\times3 = 33$ basis states, sufficient to replace the 33 $Y_{16}^m(\theta,\phi)$'s as a complete basis set. We find that the structure of Fig. 7, which was obtained by minimization of the Landau-Brazovskii free energy, consists of a linear combination of three densities corresponding to two instances of A_1 and one instance of A_2. The structure thus can also be described as having distorted octahedral, or cubic, symmetry.

III. ICOSAHEDRAL ORDERING IN THE $l = 15 + 16$ COMPOSITION SPACE

At this point, LB theory does not account for the stability of the parvovirus whose capsid has a density that closely resembles the $l = 15$ icosahedral spherical harmonic $\mathcal{Y}_{15}(h)$, which we found to be unstable. In this section we go beyond standard Landau theory by allowing the order-parameter to be described by more than one irrep and hence by multiple l.

The fact that free energies minimization can lead to coupling between different irreducible representations was noted by Dimmock [32] and others [33, 34]. A primary order parameter associated with one irrep can entrain a secondary order parameter associated with a different irrep. This can happen because the non-linear terms in the Landau energy may produce terms that are linear in the secondary order parameter times an (integer) power of the primary order parameter. Alternatively, at an accidental degeneracy point the uniform state may lose stability simultaneously against two different irreps. Multiple irreps also have been used in the context of the application of the LB free energy to block copolymers [35].

For the present case, mixing two states with different l values is in fact natural near the points along the k_0R axis that mark the borders between the stability segments of l and $l+1$. For $l = 15$ and $l = 16$, the point where $t_{15} = t_{16}$ is at $k_0R = 16$. More generally, if an odd l segment supports an icosahedral state then l can be expressed as $l = 15+6j+10k$ for certain integers j and k. The adjacent segment at $l + 1 = 6(j + 1) + 10(k + 1)$ then necessarily obeys the condition for an even l segment to be able to support an icosahedral state. Every odd l segment that supports an icosahedral state is thus bordered at $k_0R = l + 1$ by an even $l + 1$ segment that also supports an icosahedral state. Note that this is *not* the case for even l: the $l = 6$, $l = 10$, and $l = 12$ icosahedral states do not have icosahedral neighbors.

A. Composite icosahedral order parameters.

Consider the space formed by the composition of the $l = 15$ and $l = 16$ subspaces. In this extended space, icosahedral density modulations can be expressed as

$$\rho(\zeta,\xi) = \zeta\mathcal{Y}_h(15) + \xi\mathcal{Y}_h(16), \tag{14}$$

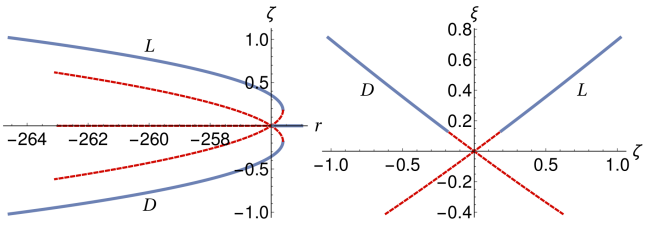

FIG. 9. Solution branches of Eq. 32 for $k_0 = 16$, u = -10, $w = 10$ that have stable sections. Stable sections of the branch are shown in blue, unstable sections in red. (left) Coefficient ζ of $\mathcal{Y}_h(15)$ as a function of the control parameter r. The two branches marked D and L are degenerate. (right) Coefficient ξ of $\mathcal{Y}_h(16)$ as a function of ζ for varying r.

This density is characterized by the *pair* of order-parameter amplitudes ζ and χ. When this ansatz is inserted into the LB free energy density and minimized with respect to the pair (ζ, ξ) then the free energy is found to have an extremum when (ζ, ξ) obeys the pair of coupled cubic equations [36]:

$$t_{16}\xi + u_1\xi^2 + u_2\zeta^2 + v_1\xi^3 + v_2\xi\zeta^2 = 0, \tag{15a}$$

$$t_{15}\zeta + u_3\xi\zeta + v_3\zeta^3 + v_4\zeta\xi^2 = 0, \tag{15b}$$

A numerical solution of the pair of coupled equations at $k_0R = 16$ is shown in Fig. 9 which shows the order-parameter pair ζ, ξ for two degenerate solution branches, marked D and L that are related under inversion when $\zeta \to -\zeta$ and $\xi \to \xi$. The superposition state is thus neither even nor odd under inversion. Note the resemblance of Fig. 9A with Fig. 5, suggestive of a first-order transition. Fig. 9B shows that ζ and ξ are comparable in magnitude and (approximately) proportional to each other.

B. Stability Diagrams.

The stability of the 15 + 16 superposition state was examined, as before, by computing the eigenvalues of the 64×64 Hessian matrix. We found that in the (r, k_0R) plane there indeed is an area near $k_0R = 16$ where the superposition state has positive eigenvalues (plus the usual three zero eigenvalues). This is shown in Fig. 10. The icosahedral state has no negative eigenvalues inside the area bordered by the solid blue lines. The diagram shows that if, for fixed r, the dimensionless radius of curvature k_0R is increased from the lower stability of the mixed state to the upper stability limit then the icosahedral state changes from "15-like", with 60 maxima, to "16-like" with 72 maxima with the new maxima appearing at the twelve 5-fold sites. The stability of icosahedral states around $k_0R = 16$ could be conceived as a form of "interference" between the $l = 15$ minimum energy state, which has a single five-fold axis, and the $l = 16$ minimum energy state which has four three-fold axes. The icosahedral state is then a compromise that allows both types of symmetry to coexist in one structure. The dashed lines give the locus of points where the uniform state acquires negative eigenvalues. The dashed and solid lines coincide along the central section, which means that along this section there could in principle be a continuous transition from a uniform to an icosahedral state.

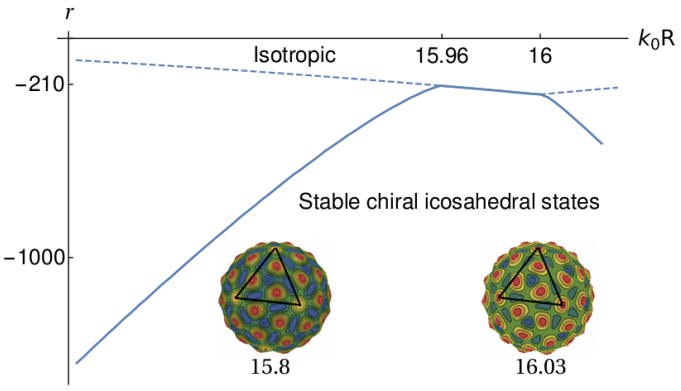

FIG. 10. Stability diagram of the $l = 15 + 16$ superposition state in the r, k_0R plane near $k_0R = 16$ with r the global control parameter. Solid blue lines: locus of points where the superposition icosahedral state acquires negative eigenvalues. Dashed lines: locus of points where the uniform state acquires negative eigenvalues. The densities of two states with different k_0R at the opposite stability limits are shown.

Enlarged views of the central section of the stability diagram are shown in Fig. 11 We introduced here the new variables t and Δ such that the reduced temperature in the $l = 15$ sector equals $t_{15} = t - \Delta$ and that in the $l = 16$ sector $t_{16} = t + \Delta$. The linear stability thresholds $t_{15} = 0$ and $t_{16} = 0$ of the uniform phase are thus $t = \Delta$, respectively, $t = -\Delta$. In terms of r, k_0 and R the new variables can be expressed as $t = r + [(k_0R)^4 - 256(k_0R)^2 + 65792]/R^4$ and $\Delta = [-16(k_0R)^2 + 8192]/R^4$. In Fig. 11, the solid red line is the stability threshold of the uniform phase. The inset shows that in the narrow sliver between the solid red and dashed blue lines, the minimum free energy state has tetrahedral symmetry. Figure 12 shows that this tetrahedral state differs from the minimum energy state in the $l = 16$ sector. The tetrahedral density is shown along one of the four triangular faces. The tetrahedral sliver disappears near $\Delta = -14$.

C. First-order and second-order transitions.

By combining the stability diagram with numerical calculation of the free energy one can determine the order of the various transitions in Fig.11. We start with the solid black line for positive Δ and negative t. The minimum free energy state in the non-icosahedral sector on the right side of the icosahedral sector is identical to the

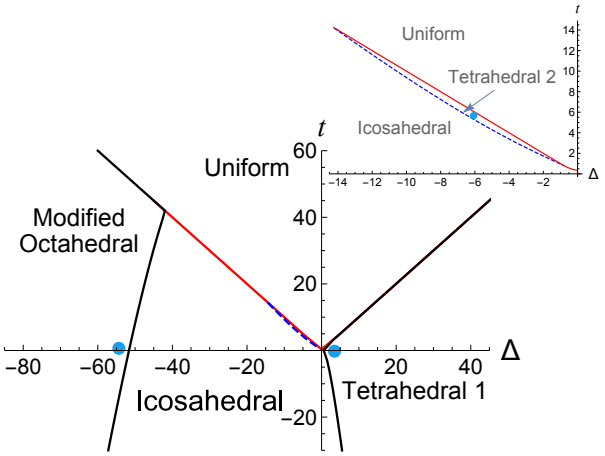

FIG. 11. Enlarged view of the central section of the stability diagram of the $l = 15 + 16$ superposition state near $k_0R = 16$. The variables t and Δ are defined by the conditions that $t_{15} = t - \Delta$ and $t_{16} = t + \Delta$. The two non-icosahedral modulated states have here tetrahedral or modified octahedral symmetry. The two black lines bordering the icosahedral sector are *spinodal lines* with lines of first-order transitions tracking the spinodal lines just inside the icosahedral sector (not shown). The red line *outside* the boxed sector indicates a line of continuous phase transitions between the isotropic and icosahedral states. The inset shows an enlarged view of the boxed sector when a tetrahedral state interposed between the isotropic and icosahedral states. Here, the red line is the stability limit of the uniform state. Blue dots: states whose densities are shown below.

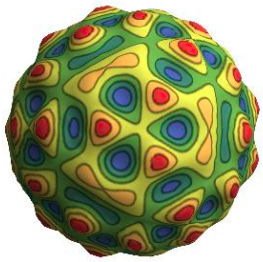

FIG. 12. Tetrahedral density, denoted "Tetrahedral 2" in Fig. 11, corresponding to $\Delta = -6$ and $t = -5.7$, inside the tetrahedral strip in the stability diagram shown along one of the three-fold axes (blue dot)

tetrahedral $l = 16$ state that was discussed in the previous section. The density corresponding to the blue dot in that sector near $t = \Delta = 0$ in Fig. 11 was already shown in Fig. 7. Figure 13 shows the difference δF between the lowest free energy state and the icosahedral free energy as a function of Δ for fixed $t = -0.1$.

For $\Delta \lesssim 0.3$ the free energy difference is zero, meaning that the icosahedral state has the lowest free energy. For $\Delta \gtrsim 0.3$, the tetrahedral state has a lower free energy with δF going continuously to zero. This is the thermodynamic signature of a first-order phase transition. The

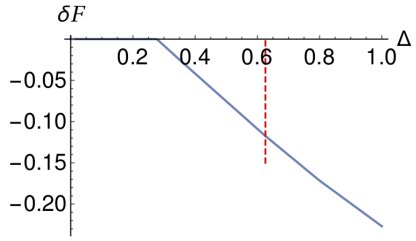

FIG. 13. Free energy difference δF between the lowest free energy state and the icosahedral free energy as a function of Δ for fixed $t = -0.1$. The red dashed line shows the stability limit of the icosahedral state

icosahedral state acquires negative eigenvalues at the red dashed line, which thus corresponds mathematically to a saddle-point and physically to a *spinodal point*. The solid black line in the stability diagram thus should be interpreted as a spinodal line. A line of first-order transitions runs near this spinodal line.

We next consider the solid red line outside the boxed sector in Fig. 11 with $\Delta \lesssim -14$. It denotes the joint stability limits of the icosahedral and uniform states. It is in fact a line of continuous phase transitions, notwithstanding the fact that the cubic non-linearity in the LB free energy is non-zero! It is thus indeed possible to have a continuous transition from a uniform state to a stable $l = 15$ like icosahedral state.

We saw that for $-14 \lesssim \Delta < 0$, a tetrahedral state interposes between the icosahedral and uniform states. The group-theoretical method developed in the previous section to describe instabilities of the icosahedral state can be readily extended to the $l = 15 + 16$ composition space. Using this method, we find that the tetrahedral state is a superposition of the two one-dimensional irreps A_g of the $l = 15$ and $l = 16$ subspaces plus one copy each of the two four-dimensional irreps G_g belonging to the $l = 15$ and $l = 16$ subspaces. For the case of the tetrahedral state shown in Fig. 12, A_g contributes a fraction of about 0.79 to the density while G_g contributes the remainder. Transitions from an icosahedral state to a tetrahedral state of this type have been shown to be first-order [37]. The dashed blue inside the boxed sector is thus a line of first-order phase transitions, as confirmed by Fig. 9. The point where the dashed blue line merges with the red line presumably corresponds to a *tricritical point* but we did not investigate this further.

Finally, the solid black line for negative Δ and negative t is a mirror image of the one for positive Δ: it is again a spinodal line where the icosahedral state becomes unstable. A line of first-order transitions tracks the spinodal line. But there is a surprise: the minimum free energy state is *not* the dihedral $l = 15$ minimum energy state that might have been expected. Instead, it *also* is a modified-octahedral state as shown in Fig. 14. This asymmetry is related to the fact that $l = 15$ ordering entrains $l = 16$ as a secondary order parameter through the cubic term in the free energy, which generates terms

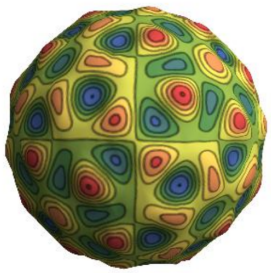

FIG. 14. Modified octahedral state corresponding to $\Delta = -65$ and $t = 0.2$ (left blue dot in Fig. 11).

that are linear in $l = 16$ and bilinear in $l = 15$. On the other hand, $l = 16$ ordering can not entrain $l = 15$ as a secondary order parameter because $l = 15$ is odd under inversion. The non-linear terms in the free energy now cannot produce terms that are linear in $l = 15$.

The entrainment of even a small amount of $l = 16$ has dramatic effects for $\Delta = -65$. If the density is decomposed as

$$\rho(\theta,\phi) = \rho_{15}(\theta,\phi) + \rho_{16}(\theta,\phi) \tag{16}$$

then the ratio $\langle\rho_{16}^2\rangle/\langle\rho_{15}^2\rangle$ of the square integrated densities in Fig. 14 is only about 2×10^{-3}. The density is principally made up of contributions from $l = 15$ spherical harmonics, as one should expect. Yet without this admixture, the state would switch back from modified octahedral to modified icosahedral state. The modified icosahedral state is recovered for $\Delta \simeq -400$.

Further decomposition in terms of the irreps of the octahedral group using the methods discuss in the previous section yields

$$\rho_{15}(\theta,\phi) = \rho_{15,A_1}(\theta,\phi) + \rho_{15,E}(\theta,\phi) + \rho_{15,F_2}(\theta,\phi) \tag{17}$$
$$\rho_{16}(\theta,\phi) = \rho_{15,A_2}(\theta,\phi) + \rho_{15,E}(\theta,\phi) + \rho_{15,F_1}(\theta,\phi) \tag{18}$$

where the symbols in the subscripts refer to the one dimensional, (A_1 and A_2), two dimensional (E) and three dimensional (F_1 and F_2) representations of the octahedral group. The relative square integrated densities contributing to the ρ_{15} term are

$$\frac{\langle\rho_{15,A_1}^2\rangle}{\langle\rho_{15}^2\rangle} = 0.0647066 \tag{19}$$
$$\frac{\langle\rho_{15,E}^2\rangle}{\langle\rho_{15}^2\rangle} = 0.326297 \tag{20}$$
$$\frac{\langle\rho_{15,F_2}^2\rangle}{\langle\rho_{15}^2\rangle} = 0.608996 \tag{21}$$

Note the small relative weight of the one-dimensional irrep A_1. The density deviates strongly from a purely octahedral structure. The relative square integrated densities contributing to the ρ_{16} term are

$$\frac{\langle\rho_{16,A_2}^2\rangle}{\langle\rho_{16}^2\rangle} = 0.114579 \tag{22}$$
$$\frac{\langle\rho_{16,E}^2\rangle}{\langle\rho_{16}^2\rangle} = 0.231169 \tag{23}$$
$$\frac{\langle\rho_{15,F_2}^2\rangle}{\langle\rho_{15}^2\rangle} = 0.654252 \tag{24}$$

This is completely different from the $l = 16$ deformed octahedral state one encounters on the right hand side of the phase diagram, which was a combination of the two one-dimensional irreps A_1 and A_2.

D. Spinodal lines and group theory

The instabilities of the $l = 15 + 16$ icosahedral state along the two spinodal lines can be analyzed by group theory. The appearance along this line of three negative eigenvalue is associated with the irrep F_{2g}. A natural choice for the eigenvectors is one with the $(1,1,1)$ direction along a three-fold symmetry direction and the $(0,0,1)$ direction along a two-fold direction. Define vectors $\vec{\eta} = (\eta_1, \eta_2, \eta_3)$ with respect to these axes. On general group-theoretic grounds, the Landau energy $\delta F(\vec{\eta})$ in this space must have the form [37]:

$$\delta F(\vec{\eta}) \propto \frac{\lambda_3}{2}|\eta|^2 + \frac{V}{4}|\eta|^4 + \frac{W}{6}|\eta|^6 + \Delta\frac{\sqrt{5}}{2}\eta_1^2\eta_2^2\eta_3^2 + \Delta\frac{\sqrt{5}}{60}(\eta_1^6+\eta_2^6+\eta_3^6) + \frac{\Delta}{4}\left(\eta_1^4(\eta_3^2-\eta_2^2) + cyclic\,perm.\right) \tag{25}$$

to sixth order in η. Here, λ_3 is the eigenvalue that changes sign at the transition while V and W are positive constants. The terms proportional to W and Δ in Eq. 25 are generated by sixth and higher order terms in ρ in the free energy functional that we did not include. $\delta F(\vec{\eta})$ describes a continuous symmetry-breaking transition that takes place at $\lambda_3 = 0$. For $\Delta = 0$, the Landau energy is $O(3)$ isotropic with arbitrary rotations in $\vec{\eta}$ space connecting degenerate states. For Δ negative, the minimum of $\delta F(\vec{\eta})$ lies along the C_3 direction and for Δ positive along the C_5 direction.

It is suggestive that the two non-icosahedral states bordering the icosahedral state in Figs. 10 and 11 should correspond to the C_5 and C_3 eigenvectors, as proposed in our first publication [23]. However, this is incorrect according to our numerical minimization results. Apparently, when the amplitude of $\vec{\eta}$ begins to grow at the instability point, this entrains other irreps. Eventually, the system evolves to the quite different tetrahedral and modified octahedral states we just discussed.

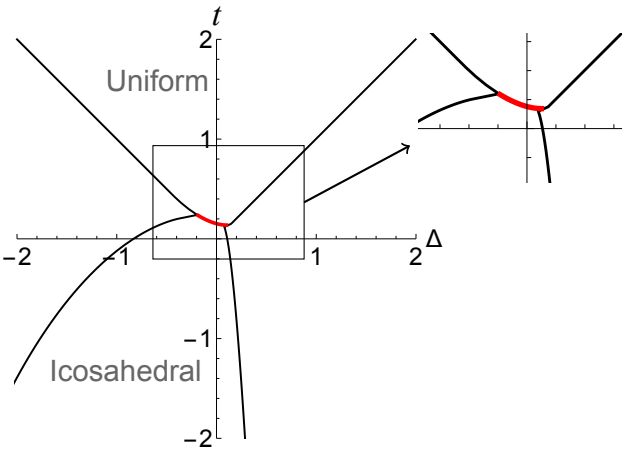

FIG. 15. Stability diagram in the $l = 25 + 26$ superposition space. The horizontal axis Δ and the vertical axis t are defined through $t_{25} = t - \Delta$ and $t_{25} = t - \Delta$. The red line is a line of first-order phase transitions from the isotropic to the icosahedral state. The two other lines bordering the icosahedral phase are spinodal lines.

E. $l = 25 + 26$

We applied the same methods to the $l = 25 + 26$ compositions space. Both $l = 25$ and $l = 26$ support icosahedral spherical harmonics but in neither case is this state stable within the LB free energy. We found that around $k_0 R = 26$ a mixed $l = 25+26$ icosahedral state can again be stable. The stability diagram, shown in Fig. 15 is quite similar to the stability diagram in the $l = 15 + 16$. However, the red line separating the icosahedral state from the uniform state now is a line of first-order transitions.

IV. CHIRAL LANDAU-BRAZOVSKII FREE ENERGY.

According to the achiral LB theory, there are two types of transitions from an isotropic to an icosahedral state. The first case is exemplied by the $l = 6, 10, 12$ and 18 cases when the transition is first-order. These icosahedral states are even under inversion and thus violate the condition of broken chiral symmetry for viral capsids. In the $l = 15 + 16$ composition space, the transition is continuous and the resulting structures have *spontaneously* broken chiral symmetry. However, spontaneous chiral symmetry breaking transition is not allowed, also because capsid proteins have intrinsic chirality. Thus, the achiral theory leads to unphysical results in either case.

In this section we generalize the LB free energy so that it can be applied to ordering transitions in systems composed of chiral units. Landau free energies for chiral materials, such as cholesteric liquid crystals [38], are constructed by obtaining the lowest-order energy density depending on ρ that transforms under inversion as a pseudoscalar density. This pseudoscalar density, multiplied by a pseudoscalar coefficient, is then to be added to the achiral free energy density constructed from scalar densities. We first construct such pseudoscalars in the large R limit – so for a flat plane – with ρ a scalar density expressed in terms of the cartesian coordinates $\mathbf{x} = (x, y)$. The chiral contribution to the free energy density f is, as usual, assumed to be local and to depend on $\rho(\mathbf{x})$ and its first and second derivatives $\nabla\rho$ and $\nabla\nabla\rho$, respectively. The chiral contribution to the free energy is

$$\Delta\mathcal{H}_\chi = \int f(\rho, \nabla\rho, \nabla\nabla\rho)\, d^2\mathbf{x}, \tag{26}$$

The symmetry group of the uniform phase in the large R limit is $SO(2) = \{\mathbf{R}_\theta | \theta \in [0, 2\pi)\}$, the group of proper rotations of the plane. The action on ρ is defined by

$$\rho(\mathbf{x}) \mapsto \rho(\mathbf{R}_\theta^T \mathbf{x}) = \rho(\tilde{\mathbf{x}}),$$

where $\tilde{\mathbf{x}} = \mathbf{R}_\theta^T \mathbf{x}$ and

$$\mathbf{R}_\theta = \begin{pmatrix} \cos\theta & -\sin\theta \\ \sin\theta & \cos\theta \end{pmatrix}.$$

The gradient vector $\nabla\rho$ and the tensor $\nabla\nabla\rho$ of second derivatives transform covariantly:

$$\nabla\rho \mapsto \mathbf{R}_\theta \tilde{\nabla}\rho,$$

$$\nabla\nabla\rho \mapsto \mathbf{R}_\theta (\tilde{\nabla}\tilde{\nabla}\rho)\mathbf{R}_\theta^T,$$

where $\tilde{\nabla}\rho = (\partial_{\tilde{x}}\rho, \partial_{\tilde{y}}\rho)$.

The free energy (26) is invariant under $SO(2)$ if the free energy density satisfies,

$$f(\rho, \nabla\rho, \nabla\nabla\rho) = f(\rho, \mathbf{R}_\theta\nabla\rho, \mathbf{R}_\theta\nabla\nabla\rho\mathbf{R}_\theta^T), \tag{27}$$

for all $\theta \in [0, 2\pi]$. Expand f as a polynomial in the six variables ρ, ρ_x, ρ_y, ρ_{xx}, ρ_{xy} and ρ_{yy}. Equation (27) then imposes constraints on the polynomial that take the form of a system of linear equations for the coefficients. Their solution give us the most general form of the invariant free density energy up to the order of the polynomial considered. For instance, at quadratic order the symmetry-restricted free energy density involves five independent terms:

$$f_2 = a_1(\Delta\rho)^2 + a_2 \det(\nabla\nabla\rho) + a_3\rho\Delta\rho + a_4|\nabla\rho|^2 + a_5\rho^2, \tag{28}$$

The subscript 2 for f reminds the reader of the order of the polynomial considered. All terms here are scalars so there are no pseudoscalar terms at quadratic order. Choosing $a_1 = 1/2$, $a_3 = k_0^2$, $a_4 = 0$ and $a_5 = (k_0^2 + r)/2$ reproduces the quadratic contributions to the LB energy density (30).

At third order we encounter one pseudoscalar term:

$$f_3 = \nabla\rho \cdot (\nabla\nabla\rho) \cdot (\mathbf{n} \times \nabla\rho),$$

where $\mathbf{n}$ is the normal to the plane (co-incident with the z-axis). This term is closely related to the Helfrich-Prost (HP) free energy density for chiral surfaces [39]. There are two fourth-order pseudoscalar terms namely

$$f_4^a = \rho\nabla\rho \cdot (\nabla\nabla\rho) \cdot (\mathbf{n} \times \nabla\rho)$$

and

$$f_4^b = \nabla\rho \cdot (\nabla\nabla\rho)^2 \cdot (\mathbf{n} \times \nabla\rho).$$

Each pseudoscalar density on a flat surfaces generates a corresponding pseudoscalar density on a curved surface that is obtained by replacing all partial derivatives by covariant derivatives and replacing $\mathbf{n}$ by the local unit normal to the surface. In Appendix B we show that the surface integrals of the covariant expressions for f_3 and f_4^a over a spherical surface are zero. Our final expression for a chiral LB free energy thus only involves f_4^b

$$\mathcal{H}_\chi = \int \left(\frac{1}{2}\Big((\Delta + k_o^2)\rho\Big)^2 + \frac{r}{2}\,\rho^2 + \frac{u}{3}\,\rho^3 + \frac{v}{4}\,\rho^4 + \chi\nabla\rho \cdot (\nabla\nabla\rho)^2 \cdot (\mathbf{n} \times \nabla\rho) \right) dS. \tag{29}$$

where χ is a pseudoscalar that measures the strength of the chiral character of the interactions between the constituent units.

In Appendix C we show that the integral

$$\int_{S^2} (\nabla Y_l^{m_1} \cdot (\nabla\nabla Y_l^{m_2}) \cdot (\nabla\nabla Y_l^{m_3}) \cdot (\mathbf{n} \times \nabla Y_l^{m_4}))\ dS = 0 \tag{30}$$

is zero for *any* set of (m_1, m_2, m_3, m_4) and *for any* l. The same is true if any of the spherical harmonics is replaced by its complex conjugate. The chiral term thus does not affect minimization of the free energy if the minimization is restricted to only one l sector.

A. Chirality and the even l icosahedral states.

We first consider the effect of the chiral term on the stable even-l icosahedral states such as $l = 6, 10, 12$. To be specific, assume that k_0R is in the interval segment $6 < k_0R < 7$ where $l = 6$ icosahedral ordering takes place such that t_6 is slightly negative while the other t_l still are positive. As before, let ξ be the $l = 6$ icosahedral order parameter. We saw that if only $l = 6$ spherical harmonics are included then the chiral term has no effect so we must allow coupling of the $l = 6$ icosahedral state to spherical harmonics with l different from $l = 6$. Since the t_5 and t_7 are the lowest t_l after t_6, these are the obvious candidates. Neither $l = 5$ nor $l = 7$ supports icosahedral order. First, minimize the free energy in the $l = 5 + 6$ composition space. Define the set c_{-m} to be the set of eleven expansion coefficients of the $l = 5$ sector with m now running from -5 to $+5$. The $l = 5$ spherical harmonics will be entrained by the $l = 6$ density if the variational free energy has terms linear in the $l = 5$ terms. In a perturbation expansion, neither the cubic nor the quartic achiral nonlinear terms can produce terms that are linear in the c_m^5 because the Y_5^m are odd under inversion while $\mathcal{Y}_h(6)$ is even. When the non-linear chiral term is computed as a mixture of the Y_5^m and the Y_6^m then the only non-zero integrals are found to be composed of one factor of $\mathcal{Y}_h(6)$ and three factors of Y_5^m, which results in a polynomial that is the sum of terms of the form $\xi c_{m1}c_{m2}c_{m3}$. Since chiral mixing produces only *cubic* terms in the c_m, $\mathcal{Y}_h(6)$ type ordering does not entrain secondary ordering of the neighboring $l = 5$ segment. The same is true for the the $l = 7$ segment. Similar conclusions are arrived at for $l = 10$ and $l = 12$.

Could the chiral term entrain other icosahedral spherical harmonics? The chiral term is found to be non-zero for combinations that are third order in $\mathcal{Y}_h(6)$ and linear in $\mathcal{Y}_h(15)$. It follows that icosahedral ordering in the $l = 6$ sector, with a density that is even under inversion, entrains $l = 15$ icosahedral ordering, with a density that is odd under inversion. The same holds for the $l = 10$ and $l = 12$ states. The chiral term thus removes the objection against icosahedral ordering in the $l = 6, 10$ and 12 segments because it generates secondary icosahedral contributions that are odd under inversion. The resulting density is neither odd nor even under inversion.

B. Chirality and the mixed $l = 15 + 16$ icosahedral state.

Now consider the effect of the chiral term on the isomeric pair of mixed $l = 15 + 16$ icosahedral states. Assume a primary icosahedral density of the form

$$\rho(\zeta, \xi) = \zeta\mathcal{Y}_h(15) + \xi\mathcal{Y}_h(16), \tag{31}$$

and minimize $\mathcal{H}_\chi$ with respect to ζ and ξ. The resulting equations are

$$(c_1{+}r)\xi{+}u_1\xi^2{+}u_2\zeta^2{+}w_1\xi^3{+}w_2\xi\zeta^2{+}\chi(3a_1\xi^2\zeta{+}a_2\zeta^3) = 0, \tag{32a}$$

$$(c_2 + r)\zeta + u_3\xi\zeta + w_3\zeta^3 + w_4\zeta\xi^2 + \chi(a_1\xi^3 + 3a_2\zeta^2\xi) = 0, \tag{32b}$$

with both a_2 and a_3 positive. Recall that for $\chi = 0$ there were two degenerate solutions (D and L) related by $\zeta \to -\zeta$. The two terms proportional to χ in the two equations lift this degeneracy. To lowest order in χ, the chiral term causes the free energy to shift by an amount $\chi\left(a_1\xi_0^3\zeta_0 + a_2\xi_0\zeta_0^3\right)$ where (ζ_0, ξ_0) denotes the $\chi = 0$ solution. Since this term is odd in ζ_0, the chiral term selects

whether the D or the L isomer has the lower free energy. Because the chiral term breaks the symmetry between the isomers, the ordering transition no longer involves unphysical chiral symmetry breaking.

C. Chirality and the uniform state.

This still leaves the uniform state. The free energy minimum in the uniform state has a density modulation $\rho = 0$ so the chirality of the uniform state cannot be determined by the properties of ρ under inversion. Instead, we can determine the chirality of the uniform state by its response to a probe that couples to density in a manner that is sensitive to the chirality of the state. From the previous arguments, it follows that to lowest order in the density ρ a local scalar chiral probe that couples to the density must have the form $\delta\mathcal{H} = -h_\chi \int f_4^b \, dS$ where h_χ is an infinitesimal chiral scalar that measures the strength of the chiral probe. The chirality M_χ of the system is defined as $M_\chi = -(d\mathcal{F}/dh_\chi)_{h_\chi=0}$ where $\mathcal{F}$ is the free energy computed from the Hamiltonian $\mathcal{H}_\chi + \delta\mathcal{H}$ that includes the probe. It is easy to see that $M_\chi = \langle f_4^b \rangle$ where $\langle .. \rangle$ indicates an average over a Boltzmann probability distribution with Hamiltonian $\mathcal{H}_\chi$. Calculating M_χ perturbatively in χ, one finds that the lowest-order non-zero contribution to M_χ is proportional to $\beta\chi\langle (f_4^b)^2 \rangle$, where the thermal average is to be computed for $\chi = 0$. Since $(f_4^b)^2$ is positive definite, this average is non-zero so the isotropic state is indeed chiral. Physically, the uniform state is chiral because thermally excited density fluctuations are chiral.

V. EXAMPLES AND CONCLUSION.

In this final section, we compare for a number of specific viral capsids the predictions of the proposed chiral Landau-Brazovskii theory with the existing Landau theory. Before doing that, we first must briefly review the Caspar-Klug (CK) classification of viral capsids [40].

A. Caspar-Klug Construction

The CK construction is based on the notion that identical capsid proteins should be distributed over an icosahedral capsid in a manner that minimizes local deformation of the proteins. Such deformations are the (unavoidable) consequence of the fact that not all sites can be symmetry-equivalent. The claim of CK theory is that such deformations are minimized by constructiing icosahedra in the manner shown in Fig. 16:

Icosahedra are generated by cutting templates from a hexagonal sheet composed of twenty adjacent equilateral triangles (see Fig. 16A). The base of each triangle is a lattice vector expressed as $\vec{A}(h,k) = h\hat{a}_1 + k\hat{a}_2$. Here $\{h,k\}$ are a pair of non-negative integers and $\hat{a}_{1,2}$ are

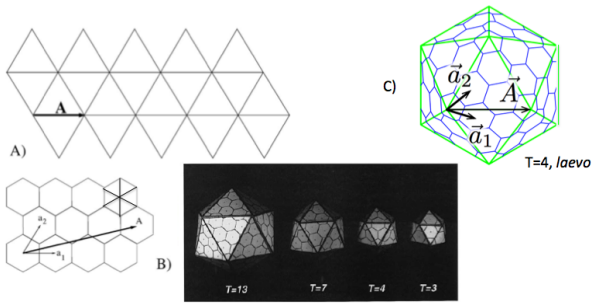

FIG. 16. Construction of icosahedra. A: A lattice vector of a two-dimensional hexagonal lattice is used to construct an equilateral triangle with vertices on lattice sites (from [41]). B: By gluing the edges of the folding template, icosahedra can be constructed ([40]). C: A $T = 7$ icosahedron with $h = 2$ and $k = 1$ is chiral.

a pair of basis vectors of the hexagonal lattice (see Fig. 16A and C). The icosahedron is constructed by pasting together adjacent exposed edges of the template (see Fig. 16B). This construction can be repeated for every pair of integers h and k. Fig. 16C shows the case of $h = 3$ and $k = 1$. The size of the icosahedron is determined by the length of the base vector $\vec{A}(h,k)$. It follows from simple geometry that twice the area per triangle $|\vec{A}(h,k)|^2$ equals $T(h,k) = h^2 + k^2 + hk$. CK icosahedra are fully characterized by this "T Number". As can be verified from Fig. 16B, CK shells are composed of 12 pentagons and $10(T-1)$ hexagons. The smallest shell is $T = 1$, composed of 12 pentagons, followed by the $T = 3$ and $T = 4$ shells shown in Fig. 16. The $T = 1$, 3 and 4 CK icosahedra are invariant under inversion. However, the two larger shells shown in Fig. 16 are the $T = 7$ and $T = 13$ icosahedra and they can be constructed in two disntict, chirally asymmetric ways that are related by inversion.

These CK icosahedra should be be compared to the Bravais lattices of solid-state physics: they are purely mathematical constructs. To produce a physical capsid, capsid proteins must be assigned to the CK icosahedra just as a "basis" of molecules must be assigned to a Bravais lattice to produce physical crystals. In the simplest case, three proteins are placed on equivalent sites of each of the triangles of Fig. 16. Capsid proteins in general have no symmetry at all and are neither even nor odd under inversion. Thus, for the T=1, 3, and 4 icosahedra, chiral proteins "decorate" achiral CK icosahedra. This extrinsic source of chirality must be distinguished from the *intrinsic* chirality of the $T = 7$ and $T = 13$ shells, which would remain chiral even for (hypothetical) capsid proteins with an inversion center. In LB theory, extrinsic chirality is generated perturbatively through the pseudoscalar term while intrinsic chirality would be produced by spontaneous chiral symmetry breaking in the absence of the pseudoscalar term.

1. *Parvovirus.*

Our first example is the parvovirus discussed before (see Fig.3). It is known to assemble reversibly from sixty monomers [20]. One thus expects that at a continuous ordering transition, sixty density maxima should evolve from the uniform state. As already noted, $\mathcal{Y}_h(15)$ describes the coarse-grained features of the measured density profile for parvovirus and it has sixty maxima. The proposed LB theory states that there *must* be a contribution to the primary order parameter that transforms as $\mathcal{Y}_h(16)$ under the symmetry operations of I. Could the amplitude ratio of the $l = 15$ and $l = 16$ contributions be obtained from a decomposition of the measured density profile into spherical harmonics? This leads to difficulties because neither $\mathcal{Y}_h(15)$ nor the $l = 15 + 16$ superposition state can describe the *fine-structure* of the parvovirus capsid. For example, the small 5-fold symmetric structures located right at the five-fold symmetry sites in Fig. 3 are not reproduced by $\mathcal{Y}_h(15)$. Density maxima located right at the five-fold sites of parvovirous have to be described by secondary order parameters represented by even-l icosahedral spherical harmonics, starting from $l = 16$. This means that it is very likely that an $l = 16$ component *would* be found in a decomposition of the density but this could not be viewed as a confirmation of the proposed theory. Fine-structure contributions to the density profile in fact have to be described by secondary order parameters, generated by higher-order non-linear terms in the density functional that are specific to parvovirus. These virus-specific secondary contributions will produce densities proportional to an integral power of the order parameter. They can be neglected close to a continuous ordering transition, as we did implicitly. The primary $l = 15 + 16$ term predicted by LB theory indeed would dominate in that case. However, experimentally measured density profiles (probably) represent density profiles quite far below the ordering transition. In that case it would be challenging to distinguish primary from secondary contributions.

The LB theory for $l = 15 + 16$ predicts that the onset of icosahedral order should either be a continuous transition – as in the existing theory – or a tetrahedral phase should intervene between the uniform and icosahedral states. Discovery of this tetrahedral phase indeed would be important evidence in favor of the LB description. This prediction is predicated on the assumption that the quartic coefficient v is positive. For negative v, additional higher-order non-linear terms have to be included. In that case, the transition is in general first order. The same reservations applies to the next cases as well.

Numerical simulations would seem to be the simplest route to test the theory. Small T=1 viruses, such as parvovirus, would be good candidates due to their small size. We mentioned that numerical simulations of coarse-grained models already have reported that capsids can assemble from a precursor condensate composed of capsid proteins that associate with genome molecules [15]. Simulations testing the theory would have to be done in the regime where the binding energy of the capsid proteins to the RNA molecule is sufficiently strong to form a globular precursor state. The proteins should have positively charged tail groups that cause the condensation of the negatively charged genome molecule(s).

2. *Picornavirus.*

Our second example concerns the *picornaviruses*, a group of animal viruses that includes the rhino and polioviruses (see Fig. 17b-c). Note that the capsid again has a pronounced chiral character. In solution, picornavirus

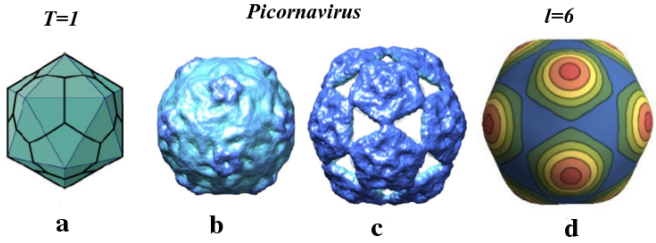

FIG. 17. (a) $T = 1$ CK construction. (b) Solution structure of native picornavirus particles (the *Equine rhinitis A* virus) and (c) the corresponding structure of the expanded particle (from ref. [42]). (d) Interpretation as an $L = 6$ orientational transition.

capsid proteins are organized into stable pentagons [9]. The pentagons are composed of five asymmetric units, each of which is composed of three proteins. In total. There are thus 15 proteins per pentagonal unit and 12 such units per capsid for a total of 180 capsid proteins. This can be indexed as a $T = 3$ CK capsid. It is however known that the pentagons survive as distinct units inside assembled picorna capsids because picorna capsid can be swollen (by chemical treatment), causing the pentagons to separately emerge while maintaining contact at their vertices (see Fig. 17c). Treating the pentagons as separate entities leads to a $T = 1$ assignment.

Treating picorna virus as an example of a T=1 capsid assembled from 12 units means that twelve density maxima should emerge at the transition. In the proposed theory, this would correspond to the $\mathcal{Y}_h(6)$ icosahedral spherical harmonic (see Fig. 17d), which is stable. If the primary order parameter is $l = 6$ then the solidification process should have the nature of a discontinuous transition. Chirality is extrinsic, i.e., imposed by the chirality of the proteins and not by the CK shell. On the other hand, the current Landau theory does not admit even l icoshaedral spherical harminics. In that case, picorna is treated as a T=3 shell with $l = 25$ and the transition should be continuous. Chirality is intrinsic in this case. There is thus a marked distinction between the two

descriptions for picorna assembly.

3. *Cowpea Chlorotic Mottle Virus.*

The Cowpea Chlorotic Mottle Virus (CCMV), a $T = 3$ RNA plant virus, is the one case for which a precursor assembly state has in fact been observed [13]. Though CCMV capsid proteins in solution are dimers, at least some fraction of the capsid proteins in the precursor state appear to be organized into *capsomers*, i.e., pentamers and hexamers of capsid proteins. Fig. 18b shows an electron micrograph of CCMV and compares it to a $T = 3$ CK organizational diagram (Fig. 18a) The capsomers

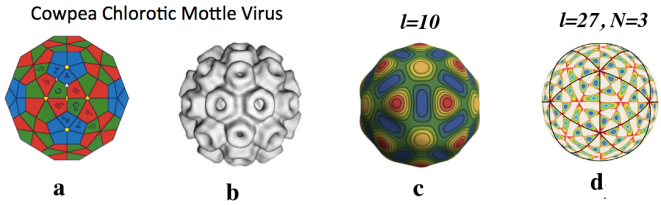

FIG. 18. (a) A $T = 3$ CK shell is divided up into twelve pentagons and twenty hexagons. Proteins are represented as kite-shaped units with 6 proteins per hexagons and 5 proteins per pentagon (b) Electron micrograph of the CCMV virus (from ref. [43]). (c) Interpretation as an $l = 10$ icosahedral spherical harmonic. (d) Interpretation as an $l = 27$ icosaehdral spherical harmonic (from ref. [5]).

are prominently visible in the assembled capsid. Other $T = 3$ *Bromoviridae* are organized in the same manner. Note that neither (a) nor (b) has an obvious chiral character. Under inversion, the representation scheme only exchanges green and red colors.

There are again two approaches possible. Assuming a CCMV capsid to be assembled from 12 pentamers and 20 hexamers, the primary $\rho(\Omega)$ of CCMV the capsomer organization should exhibit thirty two maxima. This corresponds to a $\mathcal{Y}_h(10)$ state shown in Fig. 18c. The assembly transition should be first order-and chirality is extrinsic. Alternatively, if one assumes that assembly is signaled by the development of 180 maxima then $\mathcal{Y}_h(27)$ would again be the primary order parameter density. Experimental evidence [44] indicates that the assembly of CCMV is first-order.

4. *Dengue Virus.*

The Dengue virus is a $T = 3$ RNA animal virus [45], composed of 180 subunits like CCMV but, unlike CCMV, there are no compact hexamers or pentamers in the capsid organization. There also appear to be no pentamers or hexamers in solution (Fig. 19a). The capsid is composed of elongated *dimers*, outlined schematically. Capsid proteins that border the 5-fold sites (shown as blue)

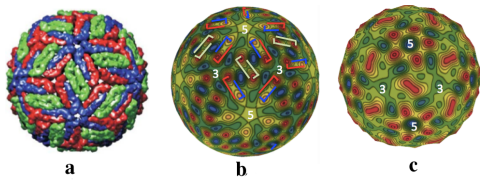

FIG. 19. (a) The Dengue virus is composed of 90 homodimers organized in a $T = 3$ lattice. The three colors correspond to the three different symmetry environments for the capsid proteins (from ref. [5]). (b) A $l = 25 + 26$ icosahedral shell. High density (red/orange) correspond to the ends of the dimers. (c) A chiral superposition state of different icosahedral spherical harmonics with 90 maxima.

dimerize with the capsid proteins that border the 3-fold sites (shown as red) The capsid proteins that occupy the 2-fold sites (green) dimerize with themselves. As noted by in ref.[5], the density of the Dengue virus capsid matches to $\mathcal{Y}_h(25)$ (see Fig. 19b, density maxima correspond to the ends of the dimers).

But there is a problem: dimers of the Dengue capsid protein are stable in solution. Assembly involves combining 90 such dimers into a capsid [46]. This suggests that the primary order parameter should have 90 maxima. However, none of the $\mathcal{Y}_h(l)$ have 90 maxima. As shown in Fig. 19c, it is possible to construct an icosahedral state with 90 maxima by superposition. The coefficients $c^2(l)$ are in this case $0.014(l = 6), 0.15(l = 10), 0.04(l = 12), 0.03(l = 15), 0.14(l = 16), 0.26(l = 18), 0.26(l = 21), 0.02(l = 22), 0.08(l = 25), 0.01(l = 26)$ (normalized to add to one) but it is unclear how such a sequence of coefficients can be generated either by LB theory or the current Landau theory. This sequence is an example of the secondary order parameter series discussed for the parvovirus case.

5. *HK97*

The HK97 virus is an extensively studied $T = 7$ bacteriophage virus [47]. Protein hexamers and pentamers are stable in solution [48] with assembled capsids formed from 60 hexamers and 12 pentamers. The initial assembly state is the "Prohead", shown in the upper left panel of Fig. 20. The hexamers of the prohead are strongly sheared [50] and have pronounced chirality. The shearing due to a net of Δ groups below the hexamers [50]. Following initial assembly, the shear strain on the hexamers is released by the scissioning of the Δ groups. The resulting "E1" state is shown in the lower panels of Fig. 20. It has only a weakly chiral character.

Figure 20 indicates that the weakly chiral E1 state can be reasonably well described by the $l = 16$ icosahedral spherical harmonic, which we found to be unstable. On the other hand, the initial assembly is into the strongly Prohead state. It is suggestive that the Prohead state is better described as an $l = 15 + 16$ stable mixed state

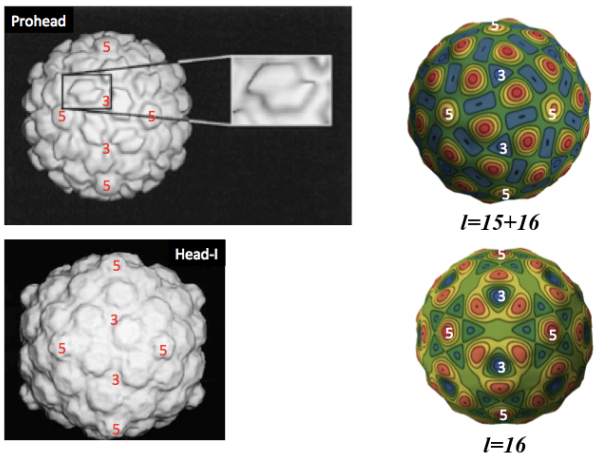

FIG. 20. Left top: Reconstruction of the first assembly stage of HK97 (Prohead 1). Three-fold and five-fold sites are indicated. The hexamers are highly sheared (from Ref.[49]). Left bottom: Reconstruction of the first EI "expanded" stage. The hexamers are symmetric. Right top: $l = 15 + 16$ icosahedral capsid near the border with the $l = 16$ sector. Right bottom: pure $l = 16$

(though the maxima of the $l = 15 + 16$ state corresponding to the hexamers are not particularly chiral). In this view, the enhanced chirality of the hexamers assists in the stabilization of the icosahedral state. Once stronger bonds have formed, the chirality can be relaxed without risk of destabilization. According to the LB theory, ordering transitions in the $15 + 16$ composition space with predominant $l = 16$ character are expected to be continuous or weakly first-order with a tetrahedral intermediate. It would be interesting to try and adjust the k_0R parameter, for example through point mutations of the Δ sections, so as to reduce the shear strain of the hexamers. The LB theory predicts that this could lead to destabilization of icosahedral shells in favor of $l = 16$ shells with tetrahedral symmetry.

HK97 is part of a family of bacteriophage and herpes viruses with double-stranded DNA genomes. In most cases, the capsids in this familiy assemble on top of a precursor spherical protein scaffold, which offer a nice realization for the supporting spherical surface assumed by the theory (HK97 is an exception).

B. Limitations

The proposed theory has obvious limitations. The assumption of the presence of a rigid spherical scaffold that stabilizes the precursor state is an example. As mentioned, there are instances for which the presence of a spherical scaffold is well-documented, such as the Herpes Simplex virus. This premise is not obviosuly valid for smaller viruses that are stabilized not by a scaffold but by *orientational interactions* between the capsid proteins. In continuum theory, such interactions can be included in a coarse-grained sense [51] by introducing a Helfrich bending energy term. In the introduction we noted that below the ordering transition, $\mathcal{H}_{LB}$ reduces to the elastic energy of a two-dimensional material with elastic moduli proportional to the square of the order parameter. If a Helfrich bending energy is added to this elastic energy, one would recovers the elasticity theory of thin shells [52]. For icosahedral shells, thin shell elasticity theory predicts a buckling transition as a function of the ratio of the 2D Young's Modulus and the bending modulus [51]. The shell should be spherical at low values of the ratio. Since the elastic moduli are proportional to the square of the order-parameter amplitude, this ratio should go to zero at a continuous ordering transition. It follows that the assumption of a spherical shell may be valid. However, preliminary work on assembly of *deformable* shells indicates that deformability has important effects. A second important limitation of the theory is the neglect of thermal fluctuations. The precursor state of CCMV reported in [13] appears to be quite non-uniform with transient protein clusters forming shell fragments. It is in fact well known that thermal fluctuations strongly affect free energy expressions of the LB form. Specifically, continuous transitions are tranformed into first-order transitions by thermal fluctuations [24]. We hope to address both questions in future work.

VI. ACKNOWLEDGMENTS

We would like to thank Alexander Grosberg for helpful discussions, the NSF for support under DMR Grant No. 1006128 and the Aspen Center for Physics for hosting a workshop on the physics of viral assembly. This paper is dedicated to the memory of our two friends and colleagues William Klug and Vladimir Lorman.

Appendix A: The irrep basis of the icosahedral group and thermodynamic stability.

In this appendix we replace the spherical harmonic basis functions with a new set associated with the irreducble representations of the symmetry group. We use it to discuss the stability of the famiiar case of the $l = 6$ icosahedral spherical harmonic.

The icosahedral group is composed of 60 rotations that map an icosahedron into itself (see Fig. 21). They fall into five classes. In the notation of Hamermesh [54] these are: the identity E with one member, two rotations about a fivefold axis, $\mathcal{C}_5, \mathcal{C}_5^4$ with 12 members, an additional two rotations about a fivefold axis, $\mathcal{C}_5^2, \mathcal{C}_5^3$ with 12 members, the rotations about twofold axes, $\mathcal{C}_2$, with 15 members, and the rotations about threefold axes, $\mathcal{C}_3, \mathcal{C}_3^2$, with 20 members. The five-fold rotations are here about the axis passing through two vertices on opposite sides of the icosahedron (see Fig. 21); the three-

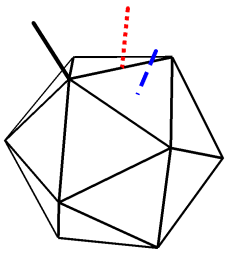

FIG. 21. The icosahedron, with examples of a five-fold, a three-fold, and a two-fold symmetry axis. The fivefold axis emerges from a vertex, the threefold axis from the center of a triangular face and the twofold axis from an edge.

fold rotations are about an axis that passes through the centers of two triangles on opposite side of the icosahedron and the two-fold rotations are through axes that pass through the center of edges on opposite sides of the polyhedron. The number of members of the five classes $1+12+12+15+20=60$ is the same as the number of elements of the group, as it should. For finite groups, the number of classes equals the number of irreducible representations (irreps) [54]. The five irreps of I are listed in table 1 of the main text where $\chi_i^{(j)}$ where $\chi_i^{(j)}$ is the character of class j for the i^{th} irrep.

Using this character table, one can project an appropriate mathematical object $\mathcal{O}$ onto a given irrep as follows:

$$\sum_{j=1}^{5} \chi_i^{(j)} \sum_{\mathbf{R}\in C_j} \mathbf{R}\cdot\mathcal{O} \tag{A1}$$

Here, $\mathbf{R}$ is one of the rotation operations of I while C_j denotes the collection of symmetry operations of the j'th class while i is the irrep in question. In the present case, the mathematical objects are the spherical harmonics belonging to a certain l. The action of the rotation operator $\mathbf{R}$ on the spherical harmonic $Y_l^m(\widehat{r})$ produces $Y_l^m(\mathbf{R}(\widehat{\mathbf{r}}))$. The rotated spherical harmonic can be expanded in the $2l+1$ spherical harmonics with the same l:

$$Y_l^m(\mathbf{R}(\widehat{r})) = \sum_{m'=-l}^{m'=+l} [D^l_{mm'}]^* Y_l^{m'}(\widehat{r}) \tag{A2}$$

Here, $[D^l_{mm'}]^*$ is the complex conjugate of an element of the Wigner D-matrix, which is readily calculated [27]. For a given l, we can, in this way, generate $2l+1$ functions of $\widehat{r}$ that transform under the symmetry operations of the group as a particular irrep of that group.

1. $l=6$

As an example, consider the case of $l=6$. Operating on the 13 functions $Y_6^m(\widehat{r})$ with Eq. (A1) for the case of the one-dimensional irrep A_g produces a 13 by 13 matrix:

$$\begin{pmatrix}
0 & 0 & 0&0&0&0 & 0 & 0&0&0&0 & 0 & 0\\
0 & \frac{84}{5} & 0&0&0&0 & -\frac{12\sqrt{77}}{5} & 0&0&0&0 & -\frac{84}{5} & 0\\
0 & 0 & 0&0&0&0 & 0 & 0&0&0&0 & 0 & 0\\
0 & 0 & 0&0&0&0 & 0 & 0&0&0&0 & 0 & 0\\
0 & 0 & 0&0&0&0 & 0 & 0&0&0&0 & 0 & 0\\
0 & 0 & 0&0&0&0 & 0 & 0&0&0&0 & 0 & 0\\
0 & -\frac{12\sqrt{77}}{5} & 0&0&0&0 & \frac{132}{5} & 0&0&0&0 & \frac{12\sqrt{77}}{5} & 0\\
0 & 0 & 0&0&0&0 & 0 & 0&0&0&0 & 0 & 0\\
0 & 0 & 0&0&0&0 & 0 & 0&0&0&0 & 0 & 0\\
0 & 0 & 0&0&0&0 & 0 & 0&0&0&0 & 0 & 0\\
0 & 0 & 0&0&0&0 & 0 & 0&0&0&0 & 0 & 0\\
0 & -\frac{84}{5} & 0&0&0&0 & \frac{12\sqrt{77}}{5} & 0&0&0&0 & \frac{84}{5} & 0\\
0 & 0 & 0&0&0&0 & 0 & 0&0&0&0 & 0 & 0
\end{pmatrix} \tag{A3}$$

One obtains results as the entries of a column vector generated by operating with this matrix on the column vector whose 13 entries are $Y_6^m(\theta,\phi)$. The column vectors that result from this operation have only three non-zero entries in the form of three function of $\widehat{r}$, the second, seventh and twelfth from the top. They are all proportional to each other and to the icosahedral spherical harmonic $\mathcal{Y}_h(6)$. This means that there is exactly one combination of $l=6$ spherical harmonics that generates a density with full icosahedral symmetry and only one instance of the one-dimensional irrep of the icosahedral group that can be constructed by this method.

Performing similar operations for the four other irreps of the icosahedral group, we find that one representative from each of three irreps can be constructed out of the $Y_6^m(\theta,\phi)$s. Those three irreps are the first three dimensional, the four dimensional and the five dimensional representation. Adding up dimensions, we have $1+3+4+5=13$ dimensions, corresponding to 13 basis states, exactly as many as are provided by the 13 spherical harmonics for $l=6$. Thus, the basis states for the irreps provide an alternative basis for the analysis of the various properties of a "crystallized" $l=6$ state. The new basis set consists of normalized basis states of the irreducible representations, $\phi_i^{(j)}(\theta,\phi)$ where the subscript refers to the representation, and the superscript in parentheses refers to the basis within the representation. In the case of the one dimensional representation, corresponding to $\phi_1(\theta,\phi)=\mathcal{Y}_h(6)$, the superscript is omitted. The normalization is

$$\int_0^{\pi}\int_0^{2\pi} \phi_i^{(j)}(\theta,\phi)^2 \sin(\theta) d\phi\, d\theta = 1 \tag{A4}$$

It is now possible to recast the Landau Hamiltonian (4) in terms of these $l = 6$ basis states. First assume that the only basis state participating is the one corresponding to perfect icosahedral symmetry, i.e. the identity irrep A_g. The effective Hamiltonian takes the usual form of a first-order transition

$$\frac{t_6}{2}a_1^2 - \frac{10u}{969}\sqrt{\frac{143}{\pi}}a_1^3 + \frac{4719v}{31280\pi}a_1^4 \tag{A5}$$

where a_1 is the amplitude of $\phi_1(\theta,\phi) = \mathcal{Y}_h(6)$. When the quadratic coefficient, t_6, is sufficiently small, a first order phase transition occurs to an ordered state, in which a_1 is non-zero; its sign is determined by the sign of the third order coefficient, u—positive for positive values of u and negative for negative u values.

Determining the stability of this state entails allowing all basis states to participate in the Hamiltonian. This expansion is greatly simplified in the irrep-based expansion because it is *entirely diagonal* so one can investigate the properties of each irrep separately. Furthermore all diagonal entries are the same for the basis states of a given irrep so can define effective temperatures $t_{6,i}$ for each irrep.

For example, if $a_5^{(i)}$ is the amplitude of a basis state of the five-dimensional irrep H_g, then the quadratic term in the expansion of the effective Hamiltonian about the ordered state has the form

$$a_5^{(i)\,2}\Big(\frac{t_6}{2} + 3a_{1,s}\frac{u}{3}\int_0^{\pi}\int_0^{2\pi}\phi_1(\theta,\phi)\phi_i^{(j)}(\theta,\phi)^2\sin(\theta)d\phi\,d\theta + 6a_{1,s}^2\frac{v}{4}\int_0^{\pi}\int_0^{2\pi}\phi_1(\theta,\phi)^2\phi_i^{(j)}(\theta,\phi)^2\sin(\theta)d\phi\,d\theta\Big) \tag{A6}$$

where only quadratic terms in the coefficient $a_5^{(i)}$ are included. The amplitude $a_{1,s}$ in (A6) is the minimizing solution to Eq. (A5). The term inside the large brackets is half the effective temperature $t_{6,5}$ associated with H_g.

The integrals in (A6) are all independent of superscript (j). If the third order coefficient u is zero and the quartic coefficient v positive, then the term in parentheses turns is positive for negative t_6 and proportional to $|t_6|$. The precise relations are listed in Table IV for the case $u = 0$. The expressions in the table hold when $t_6 < 0$, corresponding to icosahedral ordering. In the case of the one dimensional representation, the quadratic coefficient governs fluctuations in the amplitude of the icosahedral order. The fact that there are three basis states with quadratic coefficient zero reflects the invariance of the energy of an ordered state with respect to overall rotations of the density.

If u is non-zero, then the expression in parentheses are more complicated. The quadratic coefficients, $t_{5,i}$, of the $a_6^{(i)}$'s are graphed in Fig. 22, expressed in terms of their ratio with respect to u^2/v. The dashed line along the horizontal axis corresponds to the three dimensional representation and, again, reflects the fact that the density is insensitive to overall rotations of the sphere. Note that all these coefficients are either zero or positive. This means that the icosahedral state is locally stable.

TABLE IV. Values of the effective quadratic coupling for the four irreducible representations of the icosahedral group when $l = 6$ The cubic coefficient, u is equal to zero. The relationships hold when $t_6 < 0$

Irreducible representation	Quadratic coefficient, $t_{6,i}$
One dimensional, A_g	$2\|t\|_6$
Three dimensional, F_{1g}	0
Four dimensional, G_g	$(42/2299)\|t_6\|$
Five dimensional, H_g	$(2492/11495)\|t_6\|$

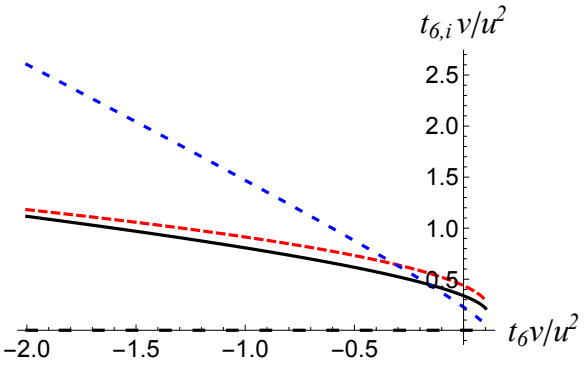

FIG. 22. The quadratic coefficients, $t_{6,i}$ when there is ordering for $l = 6$. The four curves correspond to the one dimensional representation, (straight, blue dashed), the four dimensional representation (red, dashed), the five dimensional representation (black, solid) and the three dimensional representation (dashed, along the horizontal axis).

Appendix B: Chiral terms

Without loss of generality, it is sufficient to consider the density defined on a unit sphere S^2. Let

$$I_3 = \int_{S^2}\nabla\rho\cdot\nabla\nabla\rho\cdot(\mathbf{n}\times\nabla\rho)\,dS. \tag{B1}$$

which can be expressed as:

$$I_3 = \int_{S^2}(\nabla^\alpha\rho)(\nabla_\alpha\nabla_\beta\rho)(\varepsilon^{\beta\nu}\nabla_\nu\rho)\,dS.$$

Integrating by parts,

$$I_3 = \int_{S^2}\nabla^\alpha\Big[\rho\varepsilon^{\beta\nu}\nabla_\nu\rho(\nabla_\alpha\nabla_\beta\rho)\Big] - \rho\nabla^\alpha\Big[\varepsilon^{\beta\nu}\nabla_\nu\rho(\nabla_\alpha\nabla_\beta\rho)\Big]\,dS. \tag{B2}$$

Since a sphere has no boundary, the first term is zero by divergence theorem. Expanding the second term and using the definition of the Laplace-Beltrami, $\nabla^\alpha\nabla_\alpha =: \Delta$,

$$I_3 = -\int_{S^2} \rho\Delta(\nabla_\beta\rho)(\varepsilon^{\beta\nu}\nabla_\nu\rho)+\rho(\nabla_\alpha\nabla_\beta\rho)\varepsilon^{\beta\nu}\nabla^\alpha\nabla_\nu\rho\, dS.$$

The second term involves the product of the anti-symmetric $\varepsilon^{\beta\nu}$ and the symmetric $\nabla_\alpha(\nabla_\beta\rho)\nabla^\alpha(\nabla_\nu\rho)$ and is therefore zero. Using the following identity on the unit-sphere,

$$\Delta(\nabla_\beta)\rho = \nabla_\beta(\Delta\rho) + \nabla_\beta\rho,$$

we obtain,

$$I_3 = -\int_{S^2} \rho\varepsilon^{\beta\nu}\nabla_\beta(\Delta\rho)\nabla_\nu\rho + \rho\varepsilon^{\beta\nu}\nabla_\nu\rho\nabla_\beta\rho\, dS.$$

Again, the second term in this expression is zero as it involves the product of symmetric and antisymmetric tensors. Applying the divergence theorem to the first term,

$$I_3 = \int_{S^2} (\Delta\rho)\varepsilon^{\beta\nu}\Big[\nabla_\beta\rho\nabla_\nu\rho + \rho\nabla_\beta\nabla_\nu\rho\Big]\, dS = 0,$$

where the last equality follows from the observation that the integrand is the product of symmetric and anti-symmetric tensors, thus establishing the fact that the integral of the cubic chiral term over a spherical surface is zero.

Using this same method, it can be shown that one of the two quartic chiral terms is zero:

$$I_4^a = \int_{S^2} f_4^a\, dS = \int_{S^2} \rho\nabla\rho\cdot\nabla\nabla\rho\cdot(\mathbf{n}\times\nabla\rho)\, dS = 0.$$

The only non-trivial chiral term that we find is the quartic term,

$$I_4^b = \int_{S^2} f_4^b\, dS = \int_{S^2} \nabla\rho\cdot(\nabla\nabla\rho)^2\cdot(\mathbf{n}\times\nabla\rho)\, dS. \quad \text{(B3)}$$

Appendix C: Chirality for a single irrep.

In this section we show that the if the density ρ is written in terms of a single representation expansion, i.e., if

$$\rho = \sum_{m=-l}^{l} c_m Y_l^m,$$

then the surface integral of the cubic chiral term is zero,

$$I = \int_{S^2} \nabla\rho\cdot(\nabla\nabla\rho)^2\cdot(\mathbf{n}\times\nabla\rho)\, dS = 0. \quad \text{(C1)}$$

To see this, rewrite I in its coordinate representation,

$$I = \int_{S^2} (\nabla^\alpha\nabla_\beta\rho)(\nabla^\beta\rho)(\nabla_\alpha\nabla_\nu\rho)(\varepsilon^{\nu\gamma}\nabla_\gamma\rho)\, dS.$$

Using the product rule on the first two product terms of the integrand gives,

$$I = \frac{1}{2}\int_{S^2} \nabla^\alpha(|\nabla\rho|^2)(\nabla_\alpha\nabla_\nu\varepsilon^{\nu\gamma}\nabla_\gamma\rho)\, dS.$$

Using the divergence theorem, we obtain

$$2I = \int_{S^2} \nabla^\alpha\Big[|\nabla\rho|^2(\nabla_\alpha\nabla_\nu\varepsilon^{\nu\gamma}\nabla_\gamma\rho)\Big] - |\nabla\rho|^2\nabla^\alpha[(\nabla_\alpha\nabla_\nu\rho)\varepsilon^{\nu\gamma}\nabla_\gamma\rho]\, dS.$$

Dropping the first surface term (since S^2 has no boundary) and expanding the gradient in the second term, we find

$$2I = -\int_{S^2} |\nabla\rho|^2\Big[\Delta(\nabla_\nu\rho)\varepsilon^{\nu\gamma}\nabla_\gamma\rho+\varepsilon^{\nu\gamma}(\nabla_\alpha\nabla_\nu\rho)(\nabla^\alpha\nabla_\gamma\rho)\Big]\, dS.$$

The second term, being a product of a symmetric and an anti-symmetric tensor, evaluates to zero. Using the identity, $\Delta(\nabla_\nu\rho) = \nabla_\nu(\Delta\rho) + \nabla_\nu\rho$, for unit sphere, we can rewrite the first term in previous integral as,

$$I = -\frac{1}{2}\int_{S^2} |\nabla\rho|^2\nabla(\Delta\rho)\times\nabla\rho\, dS, \quad \text{(C2)}$$

having eliminated the term involving the product $\varepsilon^{\nu\gamma}\nabla_\nu\rho\nabla_\gamma\rho$ as zero.Using the fact that if $\rho = \sum_{m=-l}^{l} c_m Y_l^m$ then $\Delta\rho = -l(l+1)\rho$ it follows that, due to the cross product term in the integrand, the integral (C2) evaluates to zero.

This proof breaks down for an enlarged composition space containing multiple irreps. For instance, if

$$\rho = \xi\mathcal{Y}_h(16) + \zeta\mathcal{Y}_h(15),$$

the direct integration shows that I is not zero.

[1] L. Onsager, Ann. NY Acad. Sci. **51**, 627 (1949).
[2] E. Kats, V. Lebedev, and A. Muratov, Physics Reports **228**, 1 (1983).
[3] P. Steinhardt, D. Nelson, and M. Ronchetti, Phys. Rev. B **28**, 784 (1983).
[4] P. C. Matthews, Nonlinearity **16**, 1449 (2003).

[5] V. Lorman and S. Rochal, Physical Review B **77**, 224109 (2008).
[6] V. Lorman and S. Rochal, Physical Review Letters **98**, 185502 (2007).
[7] R. H. Cheng, V. S. Reddy, N. H. Olson, A. J. Fisher, T. S. Baker, and J. E. Johnson, Structure **2**, 271 (1994).
[8] T. Yamamoto and S. A. Safran, Soft Matter **8**, 5439 (2012).
[9] J. Johnson, J. Tang, Y. Nyame, M. Willits, D.and Young, and A. Zlotnick, Nano Lett. **5**, 765 (2005).
[10] R. Zandi, P. van der Schoot, D. Reguera, W. Kegel, and H. Reiss, Biophys. J. **90**, 1939 (2006).
[11] A. Morozov, R. Bruinsma, and J.Rudnick, J. Chem. Phys. **131**, 155101 (2009).
[12] T. Hu and B. Shklovskii, Phys. Rev. E **75**, 051901 (2007).
[13] R. Garmann, M. Comas-Garcia, A. Gopal, C. Knobler, and W. Gelbart, J. Mol. Biol. **426**, 1050 (2013).
[14] R. Bruinsma, M. Comas-Garcia, R. Garmann, and A. Grosberg, Physical Review E **93**, 032405 (2016).
[15] O. Elrad and M. Hagan, Physical Biology **7**, 045003 (2010).
[16] F. Klein, *Lectures on the icosahedron.* (Dover Phoenix Editions, 1913).
[17] M. Golubitsky, I. Stewart, *et al.*, *Singularities and groups in bifurcation theory*, Vol. 2 (Springer Science & Business Media, 2012).
[18] M. Jaric, Phys. Rev. Lett. **55**, 607 (1985).
[19] T. Baker, N. Olson, and S. Fuller, Microbiology and Molecular Biology Reviews **63**, 862 (1999).
[20] T. Tsao and et al., Science **251**, 1456 (1991).
[21] All results in this paper are restricted to mean-field theory, and may be subject to corrections due to thermal fluctuations.
[22] A. N. Collins, G. Sheldrake, and J. Crosby, **2** (1997).
[23] S. Dharmavaram, F. Xie, W. Klug, J. Rudnick, and R. Bruinsma, EPL (Europhysics Letters) **116**, 26002 (2016).
[24] S. Brazovskii, Zh. Eksp. Teor. Fiz **68**, 175 (1975).
[25] A. Pezzutti, D. Vega, and M. Villar, Phil. Trans. R. Soc. A **369**, 335 (2011).
[26] D. Sattinger, Journal of Mathematical Physics **19**, 1720 (1978).
[27] E. P. Wigner, *Group theory and its application to the quantum mechanics of atomic spectra*, expanded and improved ed., Pure and applied physics, (Academic Press, New York,, 1959) p. 372 p.
[28] We use here a normalization for $\mathcal{Y}_h(15)$ such that $\mathcal{Y}_h(15)$ is real while $\int d\Omega\, \mathcal{Y}_h(15)\mathcal{Y}_h(15)^* = 2500/667$.
[29] See Appendix A.
[30] H. S. M. Coxeter, *Regular polytopes*, 3rd ed. (Dover Publications, New York,, 1973).
[31] J. S. Lomont, *Applications of finite groups* (Dover Publications, New York, 1993) pp. xi, 346 p.
[32] J. O. Dimmock, Physical Review **130**, 1337 (1963).
[33] E. Domany, M. Schick, J. Walker, and R. Griffiths, Physical Review B **18**, 2209 (1978).
[34] E. Domany and M. Schick, Physical Review B **20**, 3828 (1979).
[35] I. Hamley and V. Podneks, Macromolecules **30**, 3701 (1997).
[36] $t_{16} = ((k_0R)^2 - 16\times 17)^2 + r$, $t_{15} = ((k_0R)^2 - 15\times 16)^2 + r$, $a_1/16 = -80.4$, $a_2/16 = -3084.1$, $u_1 = 0.13494u$, $u_2 = 0.234946u$, $v_1 = 1.04204w$, $v2 = 0.681228w$, $u_3 = 0.623577u$, $v_3 = 0.789107w$, and $v_4 = 0.904033w$.
[37] R. Hoyle, Physica D **191**, 261 (2004).
[38] P. de Gennes and J. Prost, *Physics of Liquid Crystals* (Oxford, 1993).
[39] W. Helfrich and J. Prost, Phys. Rev. A. **38**, 3065 (1988).
[40] D. L. Caspar and A. Klug, in *Cold Spring Harbor symposia on quantitative biology*, Vol. 27 (Cold Spring Harbor Laboratory Press, 1962) pp. 1–24.
[41] T. Nguyen, R. Bruinsma, and W. Gelbart, Physical Review E **72**, 051923 (2005).
[42] S. E. Bakker, E. Groppelli, A. R. Pearson, P. G. Stockley, D. J. Rowlands, and N. A. Ranson, Journal of virology **88**, 6093 (2014).
[43] L. O. Liepold, J. Revis, M. Allen, L. Oltrogge, M. Young, and T. Douglas, Physical biology **2**, S166 (2005).
[44] G. Tresset, J. Chen, M. Chevreuil, N. Nhiri, E. Jacquet, and Y. Lansac, Phys. Rev. Applied **7**, 014005 (2017).
[45] R. J. Kuhn, W. Zhang, M. G. Rossmann, S. V. Pletnev, J. Corver, E. Lenches, C. T. Jones, S. Mukhopadhyay, P. R. Chipman, E. G. Strauss, *et al.*, Cell **108**, 717 (2002).
[46] C. López, L. Gil, L. Lazo, I. Menéndez, E. Marcos, J. Sánchez, I. Valdés, V. Falcón, C. María, G. Márquez, *et al.*, Archives of virology **154**, 695 (2009).
[47] J. Conway, W. Wikoff, N. Cheng, R. Duda, R. Hendrix, J. Johnson, and A. Steven, Science **292**, 744 (2001).
[48] Z. Xie and R. Hendrix, J. Mol. Biol. **253**, 74 (1995).
[49] J. Conway, R. Duda, N. Cheng, R. Hendrix, and A. Steven, Journal of molecular biology **253**, 86 (1995).
[50] I. Gertsman, L. Gan, M. Guttman, K. Lee, J. Speir, R. Duda, R. Hendrix, E. Komives, and J. Johnson, Nature **458**, 646 (2009).
[51] J. Lidmar, L. Mirny, and D. Nelson, Physical Review E **68**, 051910 (2003).
[52] L. D. Landau and E. M. Lifshitz, *Theory of Elasticity* (Pergamon Press, 1959).
[53] M. O. Lavrentovich, E. M. Horsley, A. Radja, A. M. Sweeney, and R. D. Kamien, Proceedings of the National Academy of Sciences , 201600296 (2016).
[54] M. Hamermesh, *Group theory and its application to physical problems*, Dover books on physics and chemistry (Dover Publications, New York, 1989) pp. xv, 509 p.